Materials Today Bio 28 (2024) 101184

Contents lists available at ScienceDirect

Materials Today Bio

journal homepage: www.journals.elsevier.com/materials-today-bio

Palladium–reduced graphene oxide nanocomposites enhance neurite outgrowth and protect neurons from Ishemic stroke

Ping Wang [a,b,1], Jinling Li [a,b,1], Shuntang Li [a,b,1], Yuanyuan Liu [a,b], Jiangu Gong [a,b], Shipei He [a,b], Weifeng Wu [a,c,*], Guohe Tan [a,b,**], Sijia Liu [a,b,***]

[a] Collaborative Innovation Centre of Regenerative Medicine and Medical BioResource Development and Application Co-constructed by the Province and Ministry, Guangxi Key Laboratory of Regenerative Medicine & Guangxi Engineering Center in Biomedical Material for Tissue and Organ Regeneration &Key Laboratory of Longevity and Aging-related Diseases of Chinese Ministry of Education, Guangxi Medical University, Nanning, Guangxi, China

[b] Guangxi Key Laboratory of Brain Science & Guangxi Colleges and Universities Key Laboratory of Biological Molecular Medicine Research, School of Basic Medical Sciences, Guangxi Medical University, Nanning, Guangxi, China

[c] Department of Cardiology, The First Affiliated Hospital of Guangxi Medical University, Nanning, Guangxi, China

ARTICLE INFO

Keywords:
Pd-RGO
Neurite
Sprouting
Outgrowth
OGD/R
Ischemia/reperfusion

ABSTRACT

Currently, the construction of novel biomimetic reduced graphene oxide (RGO)-based nanocomposites to induce neurite sprouting and repair the injured neurons represents a promising strategy in promoting neuronal development or treatment of cerebral anoxia or ischemia. Here, we present an effective method for constructing palladium-reduced graphene oxide (Pd-RGO) nanocomposites by covalently bonding Pd onto RGO surfaces to enhance neurite sprouting of cultured neurons. As described, the Pd-RGO nanocomposites exhibit the required physicochemical features for better biocompatibility without impacting cell viability. Primary neurons cultured on Pd-RGO nanocomposites had significantly increased number and length of neuronal processes, including both axons and dendrites, compared with the control. Western blotting showed that Pd-RGO nanocomposites improved the expression levels of growth associate protein-43 (GAP-43), as well as β-III tubulin, Tau-1, microtubule-associated protein-2 (MAP2), four proteins that are involved in regulating neurite sprouting and outgrowth. Importantly, Pd-RGO significantly promoted neurite length and complexity under oxygen-glucose deprivation/re-oxygenation (OGD/R) conditions, an *in vitro* cellular model of ischemic brain damage, that closely relates to neuronal GAP-43 expression. Furthermore, using the middle cerebral artery occlusion (MCAO) model in rats, we found Pd-RGO effectively reduced the infarct area, decreased neuronal apoptosis in the brain, and improved the rats' behavioral outcomes after MCAO. Together, these results indicate the great potential of Pd-RGO nanocomposites as a novel excellent biomimetic material for neural interfacing that shed light on its applications in brain injuries.

1. Introduction

The nervous system, which includes the brain and spinal cord, is crucial to many biological processes, and its damage always causes physical, cognitive, and psychological impairments, especially in degenerative diseases [1,2]. Once the nerve tissue is damaged, it is very

* Corresponding author. Collaborative Innovation Centre of Regenerative Medicine and Medical BioResource Development and Application Co-constructed by the Province and Ministry, Guangxi Key Laboratory of Regenerative Medicine & Guangxi Engineering Center in Biomedical Material for Tissue and Organ Regeneration & Key Laboratory of Longevity and Aging-related Diseases of Chinese Ministry of Education, Guangxi Medical University, Nanning, Guangxi, China.

** Corresponding author. Collaborative Innovation Centre of Regenerative Medicine and Medical BioResource Development and Application Co-constructed by the Province and Ministry, Guangxi Key Laboratory of Regenerative Medicine & Guangxi Engineering Center in Biomedical Material for Tissue and Organ Regeneration & Key Laboratory of Longevity and Aging-related Diseases of Chinese Ministry of Education, Guangxi Medical University, Nanning, Guangxi, China.

*** Corresponding author. Collaborative Innovation Centre of Regenerative Medicine and Medical BioResource Development and Application Co-constructed by the Province and Ministry, Guangxi Key Laboratory of Regenerative Medicine & Guangxi Engineering Center in Biomedical Material for Tissue and Organ Regeneration & Key Laboratory of Longevity and Aging-related Diseases of Chinese Ministry of Education, Guangxi Medical University, Nanning, Guangxi, China.

E-mail addresses: wucna65@163.com (W. Wu), tanguohe@gxmu.edu.cn (G. Tan), heming_liu@163.com (S. Liu).

[1] These authors contributed equally to this work.

https://doi.org/10.1016/j.mtbio.2024.101184
Received 29 March 2024; Received in revised form 9 July 2024; Accepted 4 August 2024
Available online 13 August 2024

difficult to repair because of the poor regeneration abilities [3,4], that have been long-lasting aspirations for researchers to develop potential therapeutic strategies [5]. Neural development and neurite growth are thought to start nervous tissue repair [6,7]. Currently, numerous attempts have been made to stimulate and enhance neurite formation for brain regeneration, utilizing a variety of assays at the cellular level, such as fetal tissue and stem cell grafting, as well as at the molecular level, such as drug therapy and electrical stimulations. However, none of these therapies can fully restore seriously injured nerves. So far, the enormous potential for rationally engineered biomaterials to elicit neural growth has sparked widespread interest.

Biomimetic materials, such as carbon-based materials like graphite, graphene, and carbon nanotubes (CNTs), and charge-conducting polymers, play a key part in directing neuronal activity and repairing damaged nerve tissues by bridging material differences [8]. Among these conductive materials, graphene and its derivatives have attractive physical and chemical properties, in terms of electrical conductivity, high charge-carrier mobility, high effective surface area, good mechanical property, high flexibility, and good biocompatibility that strongly impel its application in various biomedical fields nowadays [7], providing a promising candidate for nerve tissue engineering. More recently, graphene-based carbon nanomaterial as one kind of the most widely-used 2D materials with multiple extraordinary properties, has already been applicated in nerve tissue engendering and tissue implants, including neural stem cell research [9], bio-imaging and drug delivery [10,11], neural microelectrodes [12], and so forth [13]. However, a suitable biological material should match the natural extracellular matrix's structure and biological capabilities in order offer mechanical support and control cellular activity. In recent research, substrates coated with graphene or graphene oxide (GO) have been shown to increase the vitality of various cells such as A549 cells [14,15], NIH-3T3 fibroblasts [16,17] and embryonic stem cells [18–20]. Some graphene oxide functionalized nanocomposites have high stability in physiological solutions and can significantly reduce toxic and side effects [20,21]. However, there are only a limited number of research that have reported the modification of RGO in order to stimulate neurite sprouting and growth.

As known, neurons cannot regenerate naturally and are susceptible to damage from various injuries and diseases. *In vivo*, neuronal phenotypes interact directly with 3D extracellular matrix (ECM), which is crucial to neuronal growth. Recently, converging studies described the role of the functional topological scaffolds, including hydrogel and collagen, to promote neuronal regeneration and repair, which had been successfully proven to promote the attachment and growth of neurons effectively [22]. Synthetic ECM combinations have been proposed in a number of studies as a means of enhancing or controlling neuronal adhesion and development on the surface of nanomaterials. Of particular interest is the idea of intentionally directing the geographic distribution of neurons or of guiding axonal growth [20,22]. Indeed, the graphene monolayer sheet structure has good biocompatibility and can provide better cell scaffolds, thereby increasing intracellular tension and the number of adhesion points. Thus, the surface properties of graphene make it a platform for neuronal adhesion and even induction of neurite outgrowth, to support neuronal survival especially in the treatment of acute and chronic injury. Once graphene meets the biological environment, the absorption of water molecules and proteins occurs. The wettability affects the ability of cell adhesion-mediated integrins to attach to the graphene surface, thereby determining neuronal adhesion [23,24]. However, pure graphene sheets factually are hard to simulate the microenvironment of nerve growth *in vivo* due to its inherent biological inertness and smoothness [25,26]. For instance, long-term exposure of keratinocytes to high concentrations of raw graphene can cause damage to the mitochondrial membrane and plasma membrane [27]. Thus, many researchers have modified graphene derivatives to synthesize graphene nanocomposites, such as reduced graphene oxide (RGO), which has good solution-processability and ease of functionalization, to alter the degree of surface roughness and promote neuronal adhesion and survival [28,29]. Moreover, RGO has the much higher surface oxygen content to decrease the toxicity, compared with raw graphene. Furthermore, the active component of graphene is usually supported on a carrier for increasing the activity and stability of the catalyst and the utilization of precious metals. There are recent studies based on first-principles calculations to show that palladium nanoparticles could interact with graphene more strongly, because it tends to form a 3D structure on the graphene surface [30]. Thus, as an effective catalyst for organic reactions, palladium nanoparticles may provide an ideal combination of selectivity and activity [31]. Palladium–reduced graphene oxide (Pd-RGO) nanocomposites has increased rough morphology surface and promising catalytic activity, which achieved by dispersing palladium nanoparticles on the surface of RGO to obtain enhanced electrical conductivity and zero band gap similar to metal [32]. These specific physicochemical features are vital in promoting neuronal adhesion and signal transmission. It is worth noting that impedance reduction and charge storage capacity increased of material are beneficial for neuronal growth. Therefore, the application of neural interface materials based on Pd-RGO nanocomposites will provide a good direction for the treatment of neuronal damages. However, for the regeneration and repair of damaged neurons, the potential of Pd-RGO nanocomposites has not been widely investigated so far.

Ischemic/reperfusion stroke is a devastating cerebrovascular disease with serious neuronal injuries within the brain, ranking as the most prevalent cause of mortality and disability globally. Stroke characteristics can be modeled using both *in vitro* and *in vivo* systems, enabling mechanistic research. A classic *in vitro* model for cerebral ischemia is the oxygen and glucose deprivation-reperfusion (OGD/R) cell model, which is commonly employed to mimic the conditions leading to neuronal OGD/R injury. This model allows the study of the mechanisms underlying neuronal injury that results from OGD/R [33]. Furthermore, the middle cerebral artery occlusion (MCAO) model is one of the most commonly used *in vivo* cerebral ischemia model, which is widely used in preclinical studies for the treatment of cerebral ischemia injury [34,35]. Here we explore the construction of a novel Pd-RGO nanocomposites by covalently bonding palladium nanoparticles onto RGO surfaces to enhance neurite sprouting and outgrowth for neural repairing. We firstly prepared and characterized the Pd-RGO nanocomposites, and then explore their potential effects of them on cultured primary hippocampal neurons and ischemia/reperfusion injury rats (Fig. 1). We used CCK-8 and Calcein-AM/PI staining to detect cell viability and evaluate the biocompatibility of Pd-RGO nanocomposites with neurons. The alternations of neurite growth were subsequently detected by immunofluorescence staining, as well as western blotting, after Pd-RGO nanocomposites treatment. Furthermore, we employed the OGD/R cell model to study the potential impacts and molecular processes of Pd-RGO nanocomposites on neurons suffering from OGD/R-induced neuronal damage. Finally, MCAO rat model was further used to evaluate the effect of the Pd-RGO nanocomposites on the repair of cerebral ischemic injury *in vivo*.

2. Experimental section

2.1. Animals

C57BL/6 mice (18 days pregnant) and Sprague-Dawley (SD) rats (250–300 g) were provided by the experimental animal center of Guangxi Medical University and operated in accordance with the experimental animal ethics of the university (approval number: 201,804,200). Rats were acclimatized for at least 1 week before the start of the experiments and were kept in a thermostatic room (21 ± 2 °C) under a 12-h day/night cycle with free access to food and water.

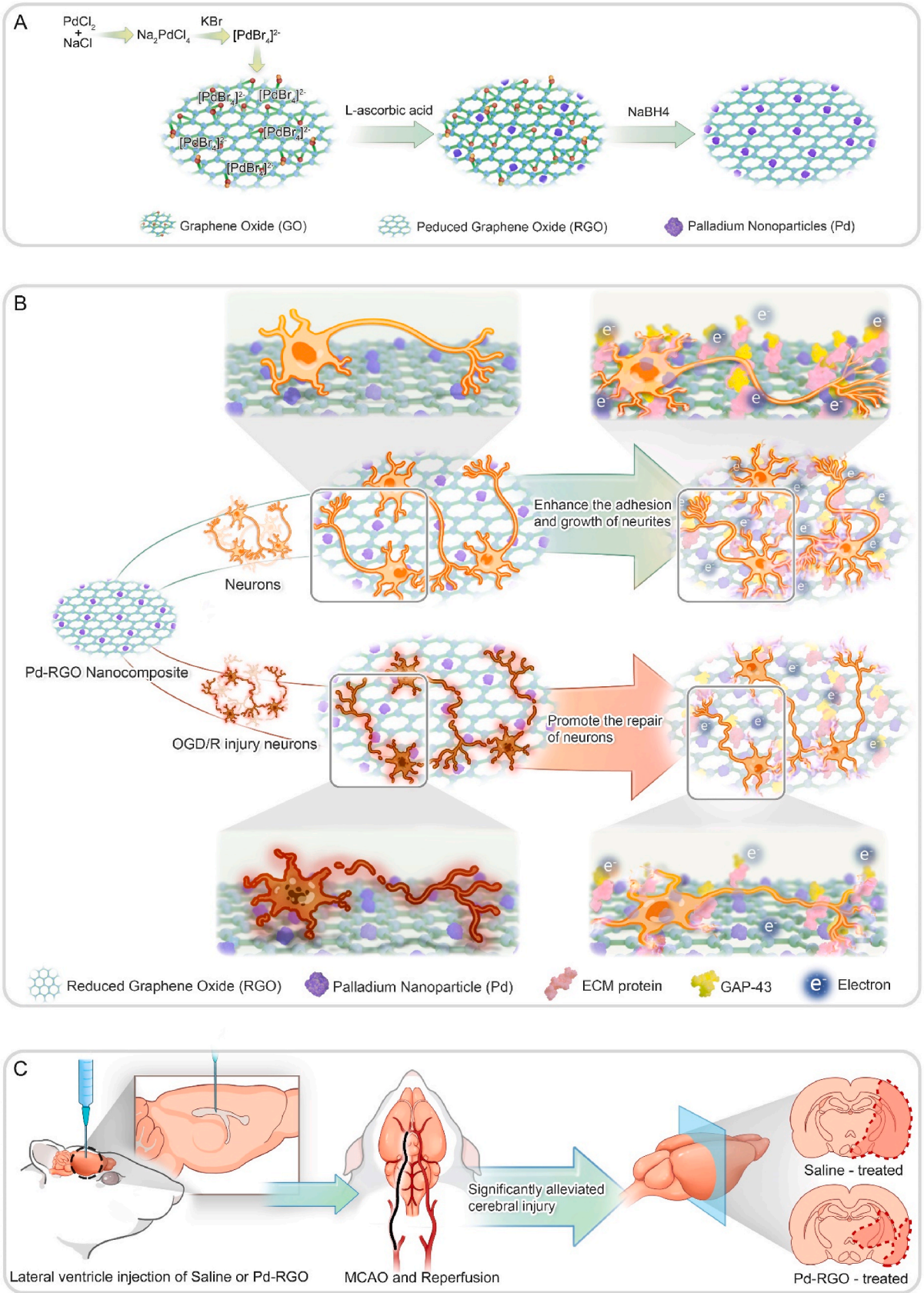

Fig. 1. A) Schematic illustration of the synthetic process of Pd-RGO nanocomposite. B) Schematic diagram depicting the influence of palladium-reduced graphene oxide (Pd-RGO) nanocomposite on the outgrowth and repair of neurons. The length and complexity of neuronal neurites are enhanced significantly by Pd-RGO nanocomposites substrate that were possibly mediated by increasing of GAP-43, matrix proteins and electrons. C) Schematic diagram of Pd-RGO composites driving neuroprotection against ischemia/reperfusion injury *in vivo* in rodent model.

2.2. Preparation and characterization of GO, RGO, and Pd-RGO nanocomposites

The modified Hummers technique was used to produce graphene oxide (GO) from graphite powder [36]. Hydrazine reduced GO at 100 °C for 24 h to produce reduced graphene oxide. Redox reactions were responsible for the formation of palladium-reduced graphene oxide (Pd-RGO) nanocomposites. Firstly, a dispersion (10 mL) of palladium chloride ($PdCl_2$) (86.4 mg) and sodium chloride (NaCl) (60 mg) was heated at 90 °C under magnetic stirring for 30 min, and then cooled to room temperature to obtain Sodium tetrachloropalladate (Na_2PdCl_4). Secondly, a dispersion (100 mL) of GO (5 mg), Na_2PdCl_4 (1 mL), potassium bromide (KBr) (70 mg), and L-ascorbic acid (18 mg) was stirred at room temperature for 6 h. Thirdly, precipitation was collected and purified by centrifugation and three-time deionized water washing. Fourthly, a dispersion (100 mL) of the precipitation obtained from the third step and sodium borohydride ($NaBH_4$) (50 mg) were stirred at room temperature for 1 h. The Pd-RGO nanocomposites were collected and purified by centrifugation, and then washed three times with ddH_2O and anhydrous ethanol, respectively. Finally, the obtained Pd-RGO nanocomposites were air-dried at room temperature in a vacuum.

All above nanomaterials were sent to Shiyanjia Lab (www.shiyanjia.com) for measurements. The transmission electron microscope (TEM) images and high resolution transmission electron microscope (HR-TEM) images were obtained using a field-emission high resolution Tecnai G2F 20 TEM (FEI, USA) with a 200 kV acceleration voltage. The sample films for TEM characterization were created by dumping a diluted Pd-RGO suspension onto a holey carbon mesh grid and air-drying at ambient temperature. The scanning electron microscope (SEM) images were obtained on a Regulus 8100 SEM (Hitachi, Japan). The sample films for SEM examination were obtained by dropping a diluted solution of Pd-RGO suspension onto a clean silicon wafer and spraying gold with the Quorum SC7620 sputtering coater after being air-dried at room temperature. The infrared absorption spectroscopic measurements were taken with GO and Pd-RGO powders, respectively, in KBr pieces, on an IS20 FTIR spectrophotometer (Thermo Nicolet, USA). X-ray diffraction (XRD) patterns of RGO and Pd-RGO samples were collected via a Miniflex-600X (Rigaku, Japan) X-ray diffractometer. X-ray photoelectron spectroscopy (XPS) spectroscopic characterization was measured on a K-Alpha X-ray photoelectron spectrometer (Thermo Scientific, USA) with a monochromatic Al Kα X-rays source at an operation voltage of 12 kV. The actual amount of Pd on Pd-RGO nanocomposites was determined by a 7700 ICP-MS (Agilent, USA). The Pd-RGO nanocomposites were treated with an acid mixture in a microwave oven setup before ICP-MS measurements. The Malvern Zetasizer Nano-ZS particle size analyzer (Malvern Instruments, UK) was used to detect zeta potential.

2.3. Preparation of glass coverslips with graphene oxide composite coating

Pd-RGO nanocomposites were ultrasonically mixed with 1 mg mL^{-1} of ethanol to create a solution for each nanocomposite. After that, a glass coverslip was coated with the sample solution. The functional Pd-RGO nanocomposites film was produced on the slide after drying at room temperature. They received a 1-h UV treatment before usage.

2.4. Primary culture of mouse hippocampus neurons

The neurons were prepared in study as described previously [37,38]. Briefly, the hippocampus was removed from the brains of day 18.5 mouse embryos. The tissues were digested with papain (Worthington) for 20 min at 37 °C. The neurons that were used to determine the viability of the cells were planted in 96-well plates, and the cells that were cultivated for western blot were cultured in six-well plates. The cells that were required for immunofluorescence were plated in 24-well plates on coverslips. To investigate the development behavior of the primary hippocampus neurons on the biomimetic nanocomposites, at least one day before culture, Pd-RGO nanocomposite group was coated with a mixed solution of Pd-RGO nanocomposite at distinct concentrations as indicated. Neurons were seeded in plating medium (Invitrogen), containing 10 % horse serum (Invitrogen), gentamicin and ampicillin, on various films with an initial density of 80,000 cm^{-2} for quantifying the survival rate of neurons cultured or detecting neurite growth *in vitro* for the indicated days. 2–4 h after planting, the original planting medium was replaced with serum-free NB/B27 medium including B27 supplement (Invitrogen), GlutaMax (Invitrogen) and Neurobasal-A medium (Invitrogen). Finally, a humidified three-gas incubator was used to grow neurons at 37 °C, using 95 % air and 5 % CO_2 [39,40].

2.5. Oxygen-glucose deprivation/re-oxygenation (OGD/R)

Phosphate-buffered saline (PBS) was used to wash the neurons, they were placed in a three-gas incubator that contained 5 % carbon dioxide, 94 % nitrogen dioxide, and 1 % oxygen for a period of one and a half hours. After replacing glucose-free DMEM with NB/B27 medium, we returned the cultured neurons to a 37 %, 5 % CO_2 humidified incubator. These neurons were stained and morphogenesis detected after 48 h.

2.6. Cell survival assay

Following a seven-day incubation period on nanocomposite films, cell viability was assessed by Cell Counting Kit-8 (CCK-8, Beyotime) and propidium iodide (PI) staining according to the protocol of the instructions. For CCK-8 detection, neurons were incubated for 4 h in diluted CCK-8 (1:10) medium, and then the absorbance at 450 nm was detected by a microplate reader. All samples were measured three replicates at a time and the experiments were repeated at least 3 times. For double-staining method of live-dead cells, Calcein-AM and PI were diluted with buffer, Neurons were submerged in the solution and incubated at 37 °C for 15 min. Calcein-AM and PI staining for live and dead were finally imaged using a fluorescence microscope.

2.7. Cytotoxicity test

Lactate dehydrogenase (LDH) is a cytoplasmic enzyme that is usually used as an indicator of cytotoxicity to assess cell damage. After cultured for 7 days, the culture media was collected to measure cellular LDH activity by measuring formazan product absorbance at 490 nm with a microplate scanner. Cell-free medium absorbance was the baseline. LDH activity in LDH release reagent-treated culture media was a high-toxicity positive control.

2.8. Western blotting

After 7 days of incubation, neurons were lysed using RIPA lysis solution containing 1 mM PMSF on ice for 1 h. Next, centrifuge the lysed mixture at 12000×*g* at 4 °C for 10 min. The BCA protein assay (Beyotime, China) and spectrophotometer assessed protein concentration A total of 50 μg of protein was separated by 10 % or 12 % SDS-PAGE at 90 V for 100 min and transferred to a PVDF membrane (Millipore USA) at 350 mA for 2.5 h at normal temperature for protein detection. After blocking the PVDF membrane with 5 % skim milk for 1 h at room temperature, primary antibodies were incubated at 4 °C for 15 h at 4 °C (rabbit polyclonal anti-MAP2, 1: 1000, Sigma; mouse monoclonal anti-β–III–tubulin, 1: 1000, Invitrogen; rabbit polyclonal anti-GAP-43, 1: 1000, Sigma; anti-GAPDH-HRP, 1 The membrane was incubated with HRP-conjugated secondary antibody at room temperature for 2 h after TBST washing. Membrane signals were detected with a chemiluminescent substrate and analyzed with ImageJ in a double-blind manner.

2.9. Immunofluorescence staining

Primary hippocampal neurons grown on coverslips were rinsed with sterile PBS and preserved with 4 % PFA at room temperature for 30 min. After washing with PBS, the neurons were incubated in 5 % BSA with 0.25 % TritonX-100 at room temperature for 1 h. Post-rinsing with PBS, neurons were incubated overnight at 4 °C with primary antibodies: rabbit polyclonal anti-Tau-1, anti-MAP2, anti-β–III–tubulin, and anti-GAP43 (Sigma, 1:500, 1:700, and 1:500, respectively). Next, Alexa Fluor 488/568/488-conjugated donkey IgG (Invitrogen, 1:2000) was employed as secondary antibodies at room temperature for 2 h. Cell nuclei were stained with Hoechst33342 (1:8000, Beyotime). The neurons were viewed under a Leica STED 660 confocal microscope (Leica, Germany). Neurolucida360 (MBF bioscience), a professional software for neuron statistics, was used to quantify the neurites from each group.

2.10. Pd-RGO preinjection

Anesthesia machine (TAIJI-IE, RWD Life Science, Shenzhen, China) sedated rats. After being profoundly sedated with 5 % isoflurane, rats were immobilized on a stereotaxic machine (68802, RWD Life Science, Shenzhen, China) and kept in oxygen with 2 % isoflurane. In rats, saline (0.9 %, 5 μL) or Pd-RGO dispersion (100 μg/mL, 5 μL) was injected into the right cerebral lateral ventricles (AP: −0.8 mm, ML: −1.4 mm, DV: −3.6 mm) using a microsyringe. The injection rate was 1 μL/min, and the needle was kept in place for 5 min after injection to promote diffusion. The needle was then gently removed for 5 min.

2.11. MCAO rat model establishment

SD rats (250–300 g) had their middle cerebral artery (MCA) blocked with a silicone rubber monofilament (Jialing Biotechnology Company, China). The right common carotid artery (CCA), external carotid artery (ECA), and internal carotid artery (ICA) were isolated and a silicone rubber monofilament was cautiously inserted into the CCA. After pushing the monofilament through the ICA and MCA, resistance was met to occlude it. The monofilament was removed after 90 min of ischemia for 24 h of reperfusion. A silicone tip obstructed the MCA. The sham group (n = 8) had no middle cerebral artery occlusion. Both Pd-RGO- and saline-treated animals were ischaemic for 90 min.

2.12. Behavioral evaluations of rats

In this study, the Zea-Longa score was used to assess the neurological deficit of rats after MCAO. The specific scoring criteria are consistent with that was described before [41,42] and the behavioral tests were performed 24 h after MCAO surgery. After behavioral testing, rats were sacrificed to gather samples for later histopathological analysis.

2.13. TTC staining

Following behavioral testing, the animal brains were collected, soaked in cold saline for 10 min, and coronally cut into five 2-mm-thick slices using Brain Matrix (RWD Life Science, Shenzhen, China). Brain slices were incubated in 2 % TTC. After 20 min of TTC solution incubation at 37 °C, sections were scanned using the GF-4AIII specimen imaging equipment. Software for ImageJ analysis was used to assess the area of infarct lesions.

2.14. H&E staining

We detected pathological alterations in rat brain tissues using hematoxylin and eosin. To clarify, rat brain tissues were kept in 4 % paraformaldehyde 24 h following MACO. After that, the samples underwent regular dehydration, embedding, and sectioning into 3 μm-thick coronal sections. Then, microscopic observation was performed using hematoxylin and eosin.

2.15. TUNEL staining

TUNEL staining was used to observe apoptosis produced by cerebral ischemia and reperfusion After being fixed for 48 h in 4 % paraformaldehyde, brain tissues were progressively moved to solutions containing 15 % and 30 % sucrose until they sank to the bottom. Brain tissues were then made into 20-μm-thick frozen sections. Antigen retrieval was performed using proteinase K, then permeabilization for 20 min in PBS containing 0.3 % Triton X-100. Following the manufacturer's instructions, coronal slices of the brain were stained using the TUNEL staining kit (Servicebio, Wuhan, China). DAPI was used to label cell nuclei for 20 min. Using an inverted fluorescent microscope, red-nucleated cells were regarded as apoptotic ones.

2.16. In vivo clearance, and toxicity of Pd-RGO

To test the *in vivo* dynamics of Pd-RGO, Pd in the brain tissues was detected by ICP-MS. Briefly, the brains of healthy rats that received lateral ventricular injections of Pd-RGO (100 μg/mL, 5 μL) were frozen at −80 °C at different time points and determined by a 7700 ICP-MS (Agilent, USA). Prior to ICP analysis, the samples were treated with a mixture of acids in a microwave oven system. To study the *in vivo* toxicity of Pd-RGO using H&E staining, healthy rats that received Pd-RGO (100 μg/mL, 5 μL) injected into the lateral ventricle of the brain were sacrificed 3 days later, and the brains were removed for H&E staining.

2.17. Quantification and statistical analysis

Image analyses were done with Image-Pro Plus 6.0 or Neurolucida360 (MBF bioscience). Western blotting band intensities were measured using IMAGE J. All statistical data were examined using SPSS 20.0 software, presenting Mean ± SEM. The quantitative data was shown as mean ± SEM. Data significance was tested using one-way ANOVA with post hoc testing. The significance threshold was 0.05.

3. Results

3.1. Characterization of the Pd-RGO nanocomposites

Firstly, we prepared and characterized the GO, RGO and Pd-RGO nanocomposites, using a series of assay including transmission electron microscopy (TEM), scanning electron microscopy (SEM), fourier transform infrared spectroscopy (FTIR), X-ray diffraction (XRD) and X-ray photoelectron spectroscopy (XPS), inductively coupled plasma mass spectrometry (ICP-MS), Zeta potential, and so on. TEM and HR-TEM images of Pd-RGO nanocomposites was shown in Fig. 2A and B. The HR-TEM image revealed that the atomic lattice fringe of Pd-RGO measured 0.22 nm, indicating an excellent match with the nominal value of Pd [43]. TEM image confirmed the uniform distribution of Pd nanoparticles in medium abundance on the RGO surface and the average particle size of approximately 180 Pd nanoparticles were 24.00 ± 0.36 (Fig. 2D). The amounts of Pd in the Pd-RGO nanocomposites were determined to be 51.20 wt% using ICP-MS characterization as shown in Tab.S1, which seems to have higher catalytic activity. SEM was performed to show that the surface of Pd-RGO nanocomposites were well-layered structure of the reduced GO sheets with a variety of Pd nanoparticles observed on the surface of RGO support. (Fig. 2C). As shown in Fig. 2E, the absorption peaks in FTIR spectrum at 1072 cm^{-1} and 1385 cm^{-1} may be caused by C–O–H vibration located on the edge of GO, the weaker absorption peak at 1730 cm^{-1} corresponds to the C=O stretching vibration of the carbonyl group, and the corresponding absorption peak of the unoxidized sp2 C=C bond is at 1622 cm^{-1}, while peaks intensity corresponding to the oxygen-containing group in

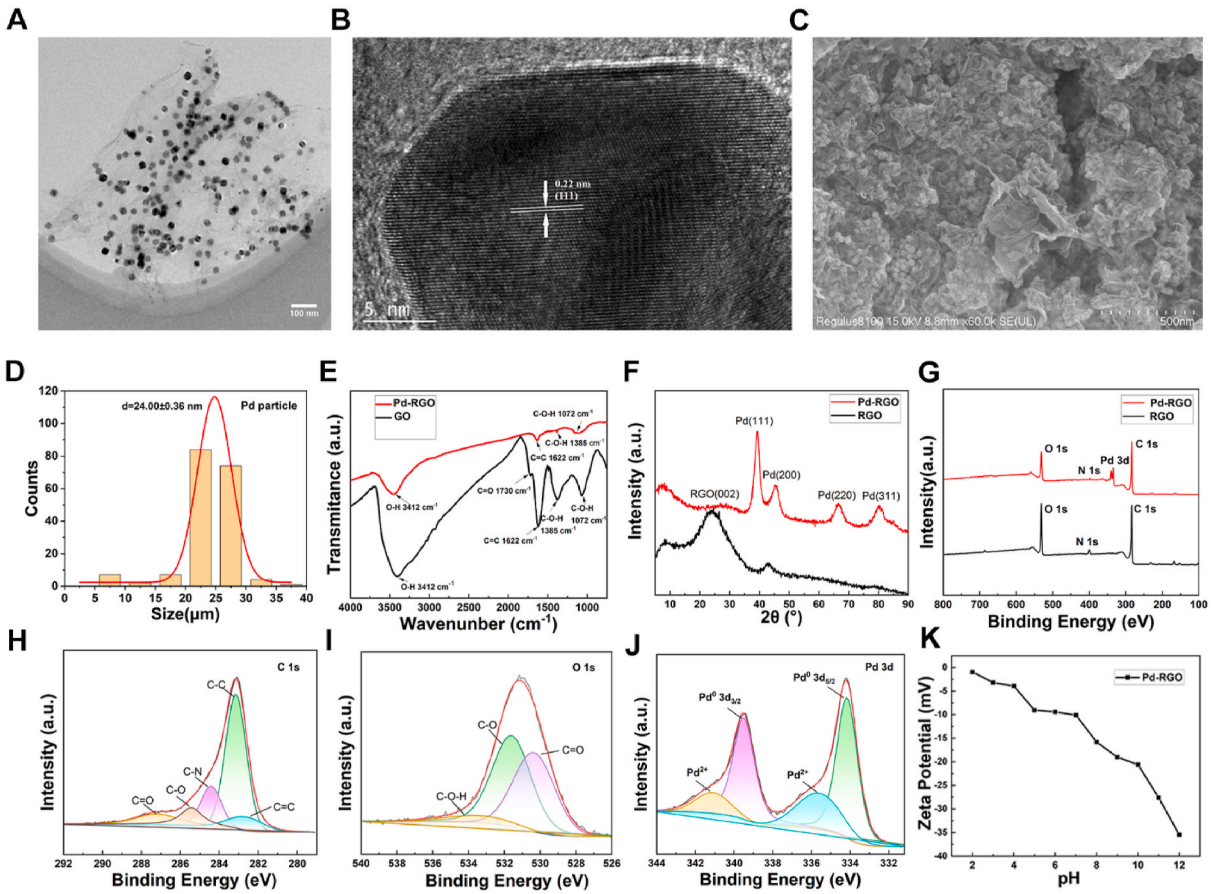

Fig. 2. Characterization of the Pd-RGO nanocomposites. A) TEM image of Pd-RGO nanocomposite, Scale bar: 100 nm; B) HR-TEM image of Pd-RGO nanocomposite, Scale bar: 5 nm; C) SEM image of Pd-RGO nanocomposite, Scale bar: 500 nm; D) Pd particle size distribution histogram; E) The FTIR Spectroscopy of GO and Pd-RGO nanocomposite; F) X-ray diffraction and G) X-ray Photoelectron Spectroscopy of RGO and Pd-RGO nanocomposites; H-J) Binding energies (eV) and deconvoluted peaks (%) for C1s, O1s and Pd 3d core levels; K) The Zeta-potential versus pH curve for Pd-RGO nanocomposites.

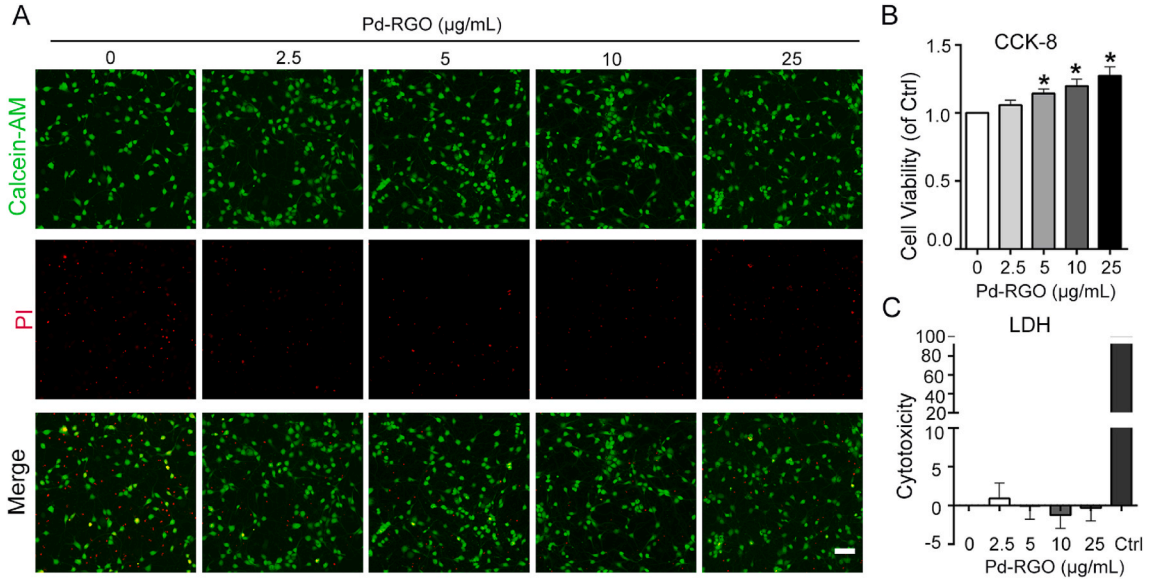

Fig. 3. Biocompatibility analysis of Pd-RGO nanocomposite. A) Calcein-AM/PI staining of live-dead cells after culturing for 7 days containing various concentrations of Pd-RGO nanocomposite ranging from 2.5 to 25 μg mL^{-1}. Living cells are green and dead cells are red. Scale bar, 50 μm. B) CCK-8 kit ($n = 9$) and C) LDH activity ($n = 7$) analysis of hippocampal neurons cultured in the 96-well plate coated with Pd-RGO nanocomposite at various concentrations of 2.5–25 μg mL^{-1} for 7 days. *$p <$ 0.05; One-way ANOVA with *post hoc* Dunnett's test.

Pd-RGO nanocomposites dramatically decreased or entirely removed, indicating most of the epoxide and hydroxyl functional groups had been successfully removed. Additionally, characteristic peaks of palladium are observed at 2θ 39.3° (111), 45.6° (200), 66.7° (220), 80.5° (311), respectively (Fig. 2F). XPS measurements showed that binding energies (eV) and deconvoluted peaks (%) for C1s, O1s and Pd 3d core levels (Fig. 2G–J). The Pd 3d XPS spectrum exhibits a pair of doublets. The peak pair seen at energy binding of 334.2 eV and 339.5 eV corresponds to Pd^0. Another peak couple was detected at 335.6 eV (Pd $3d_{5/2}$) and 341.1 eV (Pd $3d_{3/2}$) for Pd^{2+} species. The analysis of peak intensities of species revealed that Pd^0 is dominantly present in the Pd-RGO nanocomposites [44–46]. Moreover, the zeta potential diagram showed negative charges of these Pd-RGO nanocomposites (Fig. 2K).

3.2. Biocompatibility of Pd-RGO nanocomposites on cultured neurons

To investigate whether Pd-RGO nanocomposites has potential dose-dependent toxicity to the neurons [47], we isolated cultured neurons from neonatal hippocampus into 96-well plates pre-coated with Pd-RGO nanocomposites at various concentrations (Fig. 3). Calcein-AM/PI staining of live or dead cells was here used to evaluate the survival effects of cultured neurons treated by Pd-RGO nanocomposites. Within the Pd-RGO groups, we discovered that there was a significant reduction in the number of dead cells (Fig. 3A). A CCK-8 kit was then used to detect the neuronal viability *in vitro* that reveal the metabolic efficiency of the cultured neurons (Fig. 3B) [48]. Results showed that Pd-RGO nanocomposite-treated neurons, at 5, 10, 25 μg mL^{-1} concentrations, respectively, had higher viabilities than the control, suggesting that the Pd-RGO nanocomposite had a good biocompatibility. In addition, an order to evaluate the neurotoxicity of Pd-RGO nanocomposites, an investigation of LDH activity was carried out. LDH release was significantly lower than 10 % in both the Pd-RGO and control groups, and there was no discernible difference between the two (Fig. 3C). Taken above, these results indicated that Pd-RGO nanocomposites have good biocompatibility with neurons. As there was no dose-dependent toxicity observed in the experimental concentration range (2–25 μg mL^{-1}), we then choose Pd-RGO nanocomposite concentrations of 5, 10, 25 μg mL^{-1} for the subsequent experiments.

3.3. Pd-RGO nanocomposites affected axonal and dendritic morphogenesis in neurons

Neurons begin to grow neurites from the soma to the periphery after inoculation and adherence. In our study, we analyzed the neuronal morphology after 4 days of *in vitro* culture, including both average length and complexity index (NCI) of the neuronal neurites. At least 100 neurons from four independent experiments were analyzed in each group. The experimental results showed that neurons grew on the Pd-RGO nanocomposite well for 4 days, with neurites sprouting rapidly (Figs. S1A and B). As shown in Fig. S1C, the average neurite length in neurons cultured on Pd-RGO nanocomposite was longer than that in the PDL control group. Meanwhile, neurons cultured on Pd-RGO nanocomposites showed higher NCI ($p < 0.05$, Fig. S1D). These results indicate that neurons cultured on Pd-RGO nanocomposite substrates may form more complex neurites networks. Furthermore, it was interesting to note that hippocampal neurons cultured on the Pd-RGO nanocomposite substrates showed increased expression of β-III tubulin, compared to the control group (Figs. S1E and F). Thus, these findings suggest that Pd-RGO nanocomposite can promote the germination and growth of neurites in cultured neurons.

Graphene and its derivatives are intensively studied for drug/gene delivery [49], cellular imaging, and nerve repair, and regeneration [50] because of its excellent electrical characteristics and, most crucially, neuronal biocompatibility. We then examined whether Pd-RGO nanocomposite affects axonal growth or the development of dendritic morphology during neuronal development. Cultured neurons were stained with an axon-specific marker Tau-1 at DIV4 (Fig. 4A and B) and a dendritic marker MAP2 at DIV7 (Fig. 4H and I), respectively. Compared with the control group, treatment with Pd-RGO nanocomposites resulted in a significant increase in the total length of axons, number of axonal nodes, axonal complexity index and the number of axonal terminals in cultured neurons (Fig. 4C–F). This appeared to be consistent with the more significant increase in the expression of Tau-1 after Pd-RGO group treatment than that of control group (Fig. 4G). In addition, Pd-RGO nanocomposite group exhibited promoted dendrite growth, as indicated by the significant increase of the average, total dendrite length, number of dendritic nodes and dendritic complexity index (Fig. 4H–M). Furthermore, Sholl analysis demonstrated that neurons in the Pd-RGO groups were more complicated than control neurons (Fig. 4N). Subsequently, primary hippocampal neurons were cultured with Pd-RGO nanocomposites at 5, 10 and 25 μg mL^{-1} for 7 days, followed by analysis of neuronal markers MAP2. Pd-RGO nanocomposite-treated neuron has enhanced dendritic growth, as evidenced by increased expression MAP2 in western blot experiments (Fig. 4O). Taken together, these results indicate that the Pd-RGO substrates can effectively promote axonal and dendritic growth in cultured neurons.

Additionally, aiming to validate that RGO in conjunction with palladium nanoparticles can enhance its capability in promoting the growth of neuronal axons and dendrites, we further compared the efficacy of RGO with or without palladium nanoparticles in promoting neuronal growth. Compared with the control group, neurons in the Pd-RGO group had longer axons with more branches as revealed by Tau-1 fluorescence (Fig. 5A and B). RGO treatment resulted in a significant increase in the total length of axons, the number of axonal nodes, axonal complexity index and the number of axonal terminals in the cultured neurons, while Pd-RGO treatment significantly strengthen the effect of RGO treatment on neurons (Fig. 5C–F). Consistent with the statistical analysis of immunofluorescent staining, western blot results showed a similar change in the expression of Tau-1 protein of cultured neurons (Fig. 5G). To analyze the role of RGO in dendritic expansion and branching, we next stained neurons with the dendritic marker MAP2 at DIV7 (Fig. 5H and I). Interestingly, RGO substrates promoted dendritic growth of the cultured neurons above them, as evidenced by the significant increase in the total and average length of neuronal dendrites, the number of dendritic nodes and the dendritic complexity index (Fig. 5J–M). Importantly, neurons pre-treated by Pd-RGO showed much higher increase in both average and total length of dendrites than pre-treated by only RGO, indicating great potential of Pd-RGO nanocomposites in promoting neuronal morphogenesis. Furthermore, Sholl analysis revealed that cultured neurons in both Pd-RGO and RGO group were more complex than the control neurons, of which the neurons treated with Pd-RGO nanocomposites displayed most complexity among all groups (Fig. 5N). These findings confirmed the positive and promotional effect of both RGO and Pd-RGO on neurite growth of neurons.

Growth-associated protein-43 (GAP-43) is a commonly used marker for neuron growth cones [51]. In order to further explore whether the growth of neuronal neurites on Pd-RGO nanocomposite is related to the upregulation of GAP-43, we performed immunofluorescence staining and western blot experiments of neurons on the seventh day. As shown in Fig. 6A, GAP-43 fluorescence was more enriched on the Pd-RGO nanocomposite substrates, than the control. Consistent with the results of immunofluorescence staining, western blot experiments further demonstrated that the expression of GAP-43 protein in neurons grown on Pd-RGO nanocomposite were significantly increased compared to the control group ($p < 0.01$) (Fig. 6B and C). Moreover, western blot analysis revealed that there are highest levels of MAP2 and GAP-43 expression in neurons of the Pd-RGO group, compared with RGO-treated group, implying the promoting role of palladium nanoparticles (Fig. 5O and P). Together, these findings underscore the upregulation of Pd-RGO nanocomposites on GAP-43 that possibly promote neurite outgrowth.

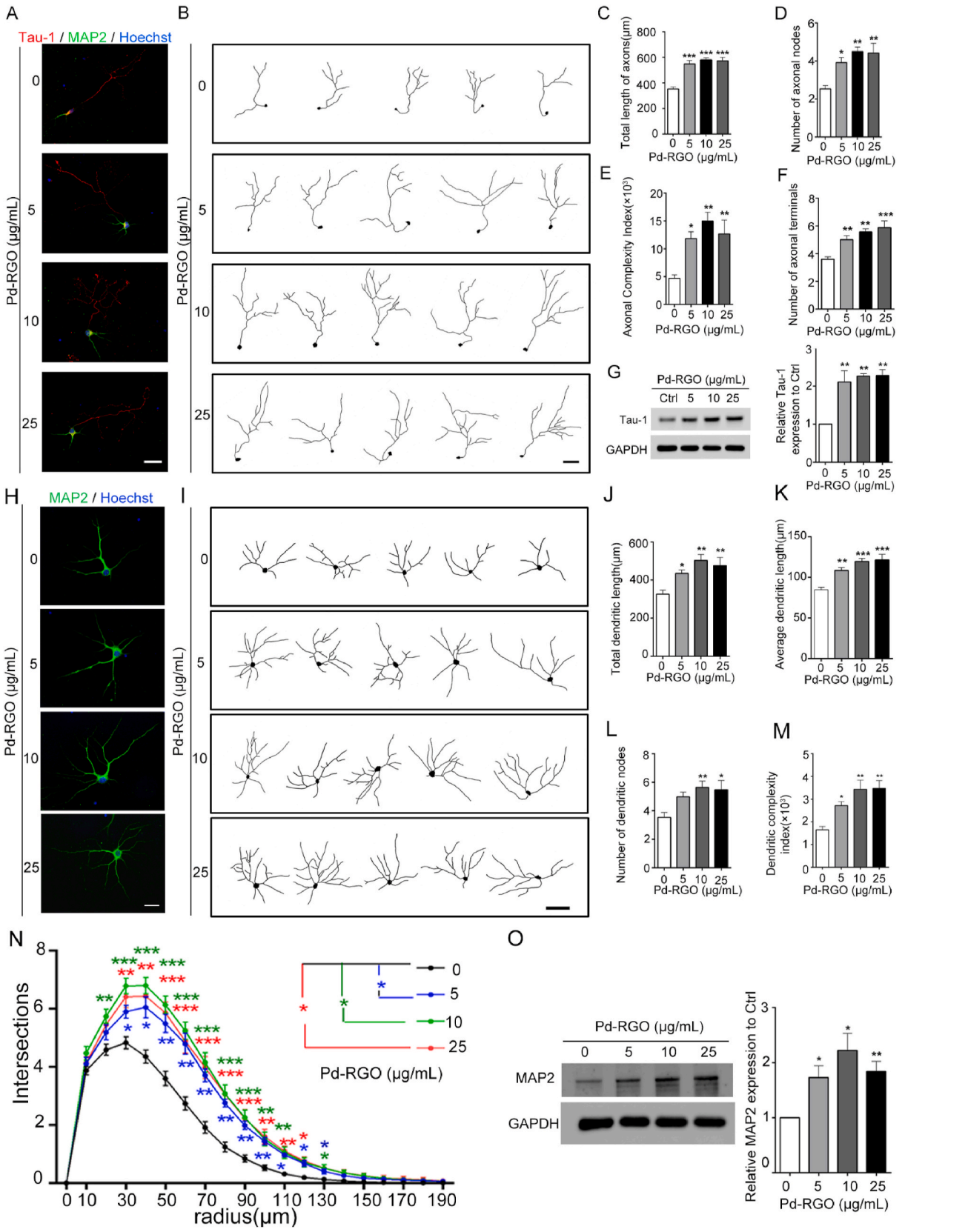

(caption on next page)

Fig. 4. Pd-RGO nanocomposite enhanced axonal and dendritic length and complexity in the neurons. A) Representative images of cultured DIV4 hippocampal neurons immune-labeled with the dendritic marker MAP2 (green), axonal marker Tau-1 (red), with counterstaining of nuclear marker Hoechst (blue). Scale bar, 50 μm. B) Sample tracings of Tau-1-immunolabeled neurons. Scale bar, 50 μm. C) Quantification of total length of axons. D) Number of axonal nodes. E) Axonal complexity index and F) Number of axonal terminals of neurons stained with axon-specific marker Tau-1 at DIV4. Data are expressed as mean ± SEM; $n = 80–140$ in each group; the experiment was repeated for five times. G) Western blot analysis of neuronal Tau-1 expression on the control group and the Pd-RGO nanocomposite groups at distinct concentrations on day 7. Quantification of the results are shown in the right. H) Representative images of cultured DIV7 hippocampal neurons. Scale bar, 50 μm. I) Sample tracings of MAP2-immunelabeled neurons. Scale bar, 50 μm. J) Quantification of total length of dendrites. K) Average length of dendrites. L) Number of dendritic nodes and M) Dendritic complexity index of neurons stained with dendritic marker MAP2 at DIV7. $n = 80–140$ in each group and were collected from six independent experiments. For *post hoc* Bonferroni tests. N) Sholl analysis quantifies dendritic complexity ($n = 80–100$ neurons *per* group, the experiment was repeated six times). O) Western blot analysis of neuronal MAP2 expression in the control group and the Pd-RGO nanocomposite groups at different concentrations on day 7. All data were shown in mean ± SEM and were collected from ten independent experiments. Data were analyzed by one-way ANOVA and compared with the control group, using *post hoc* Bonferroni post-tests. $^{*}p < 0.05$, $^{**}p < 0.01$, $^{***}p < 0.001$.

3.4. Pd-RGO nanocomposite facilitates neurite outgrowth after OGD/R injury

The OGD/R cell model is widely used for modeling the condition of neuronal damage that causes neuronal harm. Thus, we next further investigate the potential effects of Pd-RGO nanocomposite on primary neurons after exposure to OGD/R. Cell viability of the neurons was examined by Live−Dead assay, CCK-8 assay, and LDH assay. As shown in Fig. S2A, the number of dead cells detected by Live−Dead assay was much higher after OGD/R treatment than the sham control. It is worth noting that the number of dead cells decreased after Pd-RGO nanocomposite treatment. Furthermore, both the CCK-8 assay and LDH assay were conducted to further evaluate cell viability. Notably, a significant reduction in cell viability was observed following OGD/R injury ($p < 0.001$), thereby confirming the successful establishment of the OGD/R cell injury model (Figs. S2B and C). After OGD/R injury, Pd-RGO nanocomposites showed a slight tendency of a higher viability for neurons.

In order to further explore potentially affected molecules under the protective mechanism of Pd-RGO nanocomposites within neurons, we next detected MAP2, Tau-1 and GAP-43 expression in neurons exposed to OGD/R. Western blotting results showed that compared with the control group, the expression of MAP2, Tau-1 and GAP-43 in the OGD/R group was significantly reduced ($p < 0.01$), while the expression of MAP2, Tau-1, and GAP-43 in the OGD/R + 10 μg mL^{-1} Pd-RGO nanocomposite group was significantly increased ($p < 0.05$) (Fig. 7A–E). However, no significant difference was found in the OGD/R + 5 μg mL^{-1} or 25 μg mL^{-1} Pd-RGO nanocomposite groups ($p > 0.05$). To further elucidate the direct effect of Pd-RGO nanocomposite on dendritic outgrowth, we then calculated the average and total length of the dendrites, the number of dendritic nodes and the dendritic complexity after OGD/R injury. As shown in Fig. 7F–I, when compared with the control group, most dendrites of neurons in the OGD/R group were shortened, the average and total length of the dendrites was markedly decreased ($p < 0.01$). The number of dendritic nodes and the dendritic complexity were significantly decreased ($p < 0.01$) (Fig. 7J and K). While compared with the OGD/R group, the average and total length of the dendrites neurites was significantly increased in OGD/R + 10 μg mL^{-1} Pd-RGO nanocomposite group ($p < 0.01$) (Fig. 7H and I). Consistent with these results, the number of dendritic nodes and the dendritic complexity were also improved in OGD/R + Pd-RGO nanocomposite group ($p < 0.01$) (Fig. 7J and K). Furthermore, Sholl analysis revealed that neurons were less complex after OGD/R Injury, but markedly enhanced in OGD/R + Pd-RGO nanocomposite group (Fig. 7L). The above results indicate that Pd-RGO nanocomposites up-regulate the expression levels of MAP2, Tau-1, and GAP-43 in cultured neurons, and facilitate dendritic growth even after OGD/R injury, suggesting rescue effect of it on these injured neurons.

3.5. Pd-RGO protect the brain from injuries in rat model of ischemic stroke

Given the strong evidence that Pd-RGO has neuroprotective effects in repairing injured neurons *in vitro*, we subsequently assessed the efficacy of Pd-RGO in the ischemic brain *in vivo* using rat models of MCAO. Pd-RGO or saline was injected into the right ventricle of rats at 48 h before MCAO surgery-induced ischemic brain injury (Fig. 8A). Histological analysis using H&E staining in different organs showed no morphological changes or signs of inflammation observed after Pd-RGO injection (Fig. 8B), indicating the biosafety of Pd-RGO *in vivo*. Moreover, the clearance efficacy of Pd-RGO in the brain were also evaluated. Results from inductively coupled plasma mass spectrometry (ICP-MS) showed a decrease in the amount of Pd over time, indicating that Pd-RGO *in vivo* could be gradually cleared (Fig. 8C). 2,3,5-triphenyltetrazolium chloride (TTC) staining was then used to detect cerebral infarct areas, with about 37 % infarct areas in the MCAO models; in contrast, the infarcted area was significantly reduced (approximately 21 %) in rats pre-injected with Pd-RGO (Fig. 8D and E). At 24 h after the 90-min MCAO, the behavior of rats with neurological deficits was assessed by the Zea-Longa scoring. Zea-Longa scores are the most widely used indicator for evaluating neurological deficit of the rats, as followed: 0, normal neurological status; 1, mild deficit, impaired left forelimb extension; 2, moderate deficit; inability to walk straight due to lateral deviation; 3, severe deficit; inability to stand and repeated falls to the left; 4, The most severe category; loss of spontaneous locomotion and consciousness [41,42]. Surprisingly, the neurological deficit scores of the Pd-RGO treated rats were significantly reduced compared with those of the saline treated ones (Fig. 8F and G). These results suggest that Pd-RGO pretreatment reduces the infarct area after cerebral ischemia and improves motor function under brain injury.

3.6. Pd-RGO protects neuronal loss in the MCAO models

To observe the morphological alterations associated with Pd-RGO therapy, we subsequently stained rat brain tissue slices and discovered that most of the cortical areas of the ischemic hemisphere were infarcted in the saline group, whereas a significantly smaller portion was infarcted in the Pd-RGO-treated group (Fig. 9A). Of note, even in the center infarcted region, the cells exhibited only nuclear abnormalities, with neither vacuolar degeneration or cytoplasmic lysis. As mentioned above, Pd-RGO attenuated apoptosis and cell loss in the MCAO model, which contained neurons, astrocytes, and microglia. Thus, we next stained brain slices with TUNEL and DAPI to determine the amount of cell apoptosis and loss in MCAO animals. As demonstrated, Pd-RGO decreased the number of TUNEL-positive cells and preserved more DAPI-stained cells than the saline group. (Fig. 9B).

4. Discussion

Graphene oxide nanocomposites have been widely applied in the field of biosensors, but there are few studies on the potential of Pd-RGO nanocomposites for neural development and regeneration. In this study, we first explored the impact of Pd-RGO nanocomposites on neurite growth in hippocampus neurons, which are very vulnerable to a variety of environmental factors. We choose hippocampal neurons as the cell models due to their classic and specific neurite morphogenesis both *in*

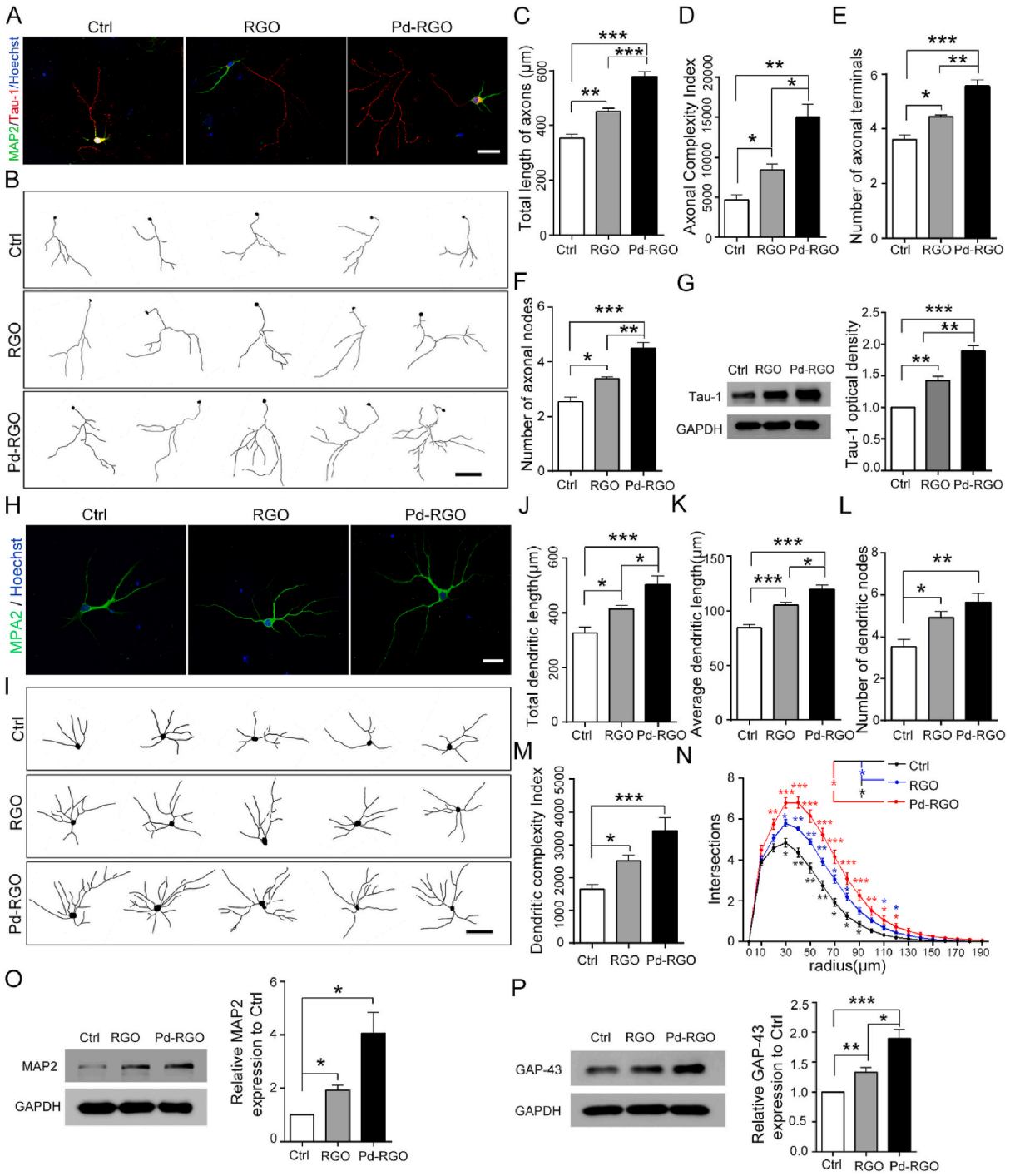

Fig. 5. Pd-RGO nanocomposites enhanced neuritic length and complexity of cultured neurons, compared with the RGO-treated group. A) Representative fluorescent images of DIV4 hippocampal neurons. Neurons were stained with Tau-1 (red) and MAP2 (green). Scale bar, 50 μm. B) Neurolucida tracings of representative Tau-1-immunolabeled neurons on day 4 after seeding. Scale bar, 50 μm. C–F) Quantification of total length of axons, axonal complexity index, number of axonal terminals and number of axonal nodes of neurons stained with axon-specific marker Tau-1 at DIV4. G) Western blot analysis of Tau-1 of hippocampal neurons on different groups and the relative optical densities ($n = 3$). H) The representative fluorescence images of neurons on various substrates on day 7 after seeding, neurons were immune-stained with and MAP-2 (green), Scale bar represented 50 μm. I) Neurolucida tracings of representative MAP2-immunolabeled DIV7 neurons. Scale bar represented 50 μm. J-M) Quantification of total length of dendrites, average length of dendrites, number of dendritic nodes and dendritic complexity index of neurons on different groups. N) Quantification of dendritic complexity as measured by Sholl analysis. O) Western blot analysis of MAP2 and P) GAP-43 of hippocampal neurons on different groups. The experiments were repeated more than five times. All Data are expressed as mean ± SEM, $n = 80$–140 neurons in each group. Data were analyzed by one-way ANOVA, with *post hoc* Bonferroni post-tests; $^{*}p < 0.05$, $^{**}p < 0.01$, and $^{***}p < 0.001$.

vivo and *in vitro* [52,53] that is closely related to neural injury and repairing [54,55]. Previous research results showed that graphene nanomaterials generally have good biocompatibility [56], which have been shown to be chemically inert, mechanically robust [57] and low-cytotoxic [58] compared with carbon nanotubes. There was no significant cytotoxicity observed, as Pd-RGO nanocomposite did not affect cell viability (Fig. 3); furthermore, coating with Pd-RGO nanocomposites could provide suitable support for neuron attachment and

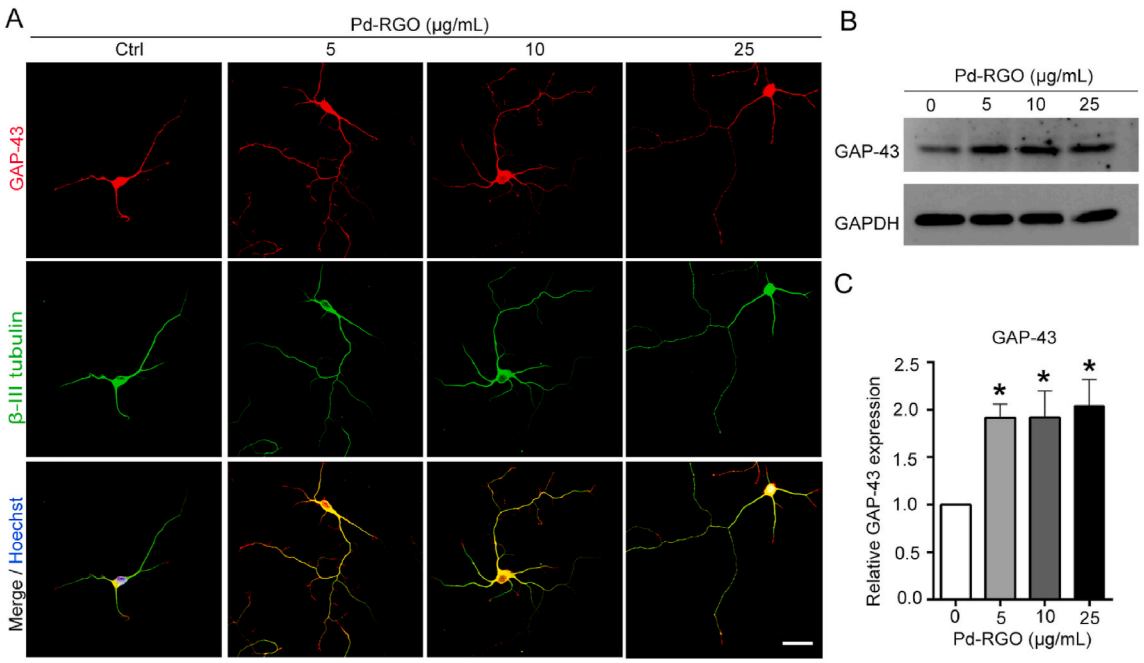

Fig. 6. The Pd-RGO nanocomposite significantly upregulated GAP-43 expression in cultured neurons. A) Representative images of primary hippocampal neurons at DIV7 immune-labeled with GAP-43 (red) and β-III tubulin (green), with counterstaining of nuclear marker Hoechst (blue). Scale bar, 30 μm. B, C) Western blot analysis (B) and the statistical results (C) of neuronal GAP-43 expression after Pd-RGO nanocomposite treatments at distinct concentrations at DIV7. Data are presented as means ± SEM. $n = 3$ for each group. $^*p < 0.05$; One-way ANOVA with *post hoc* Dunnett's test.

growth. These findings indicate that Pd-RGO nanocomposites coating may be potentially used as surface treatments for cultured neurons, suggesting a novel promising tool for promoting neuronal growth.

Injuries to the central nervous system frequently result in death or lifelong disability, particularly those caused by stroke or degenerative disorders. The response to neuronal damage is mediated by a variety of biological processes, including axonal degeneration, excitotoxicity, oxidative stress, demyelination, and inflammation [59]. As a result, neuronal injury is a complicated process that involves the simultaneous changes of the morphology, activity, and connection within the network. While there are many variables that affect the structural and functional healing of a damaged nervous system, findings from other sources support the application of graphene to promote the neurite sprouting of treated nerve cells [60]. Designing innovative therapeutics for neurological applications requires adapting the microenvironment of three-dimensional (3D) tissue scaffolds to modulate neural cell adhesion or neurite development. Here, Pd-RGO nanocomposites-built 3D scaffolds have achieved key characteristics for implantable prostheses, such as biocompatibility, microscale stability and homogeneity, conductivity, and controlled mechanical properties (Figs. 2–5, S1). These characteristics create an optimal 3D matrix for neuronal residency, guidance, extension, and regenerative outgrowth in OGD/R cell models (Fig. 7).

In the central nervous system, it is extremely difficult to repair injured neurons. It is worthy of noting that electrical stimulation is beneficial for neuronal growth and regeneration [61,62]. Many of the neural scaffolds that have been proposed are electroactive biomaterials, which allow electric current to flow through electro-conductive scaffolds and encourage neuronal development, therefore repairing or restoring damaged neurological processes. Popular possibilities for neural scaffolds include metals that are stable and resistant to corrosion, such as gold, platinum, iridium, platinum-iridium alloy, titanium, and stainless steel. Additionally, carbon nanotubes, graphene, and conducting polymers have all shown to be viable options [63–67]. However, the usage of these methods is restricted due to the fact that they need numerous stages, whilst the fabrication conditions, which include high temperatures, vacuums, or organic solvents, are detrimental to the hydrated polymer networks [68,69]. Here, we report on effectively growing neurons on Pd-RGO composites and demonstrate that these composites promote and sustain the proliferation of cultured neurons. Pd-RGO composites is a particularly promising choice for tissue engineering and prosthetics due to their high charge carrier mobility, intrinsic low electrical noise, and lower cytotoxicity when compared to RGO. The rugged and rippling structure of Pd-RGO nanocomposites may promote mechanical interlocking with hippocampal neurons and thus improved the adhesion. Moreover, the catalytic hydrogenation performance of palladium nanoparticles could increase the electrochemical capacitance of Pd-RGO nanocomposites which contributes to the electrical excitability in neurons, and thereby promote the elongation of fine neuronal processes of neurons.

Processes growing from the cell body of a neuron are called neurites that can be divided into axons and dendrites based on its length and number. In the brain, neurite germination and growth is one of the important signs that neurons begin to develop [70]. It was worth noting that hippocampal neurons grown on Pd-RGO nanocomposite substrate have longer neurites including axon and dendrite more complex neural networks, suggesting that Pd-RGO nanocomposites could effectively promote the growth and development of neurons (Fig. S1). β-III tubulin, Tau-1 and MAP2 are important components of neurite, respectively [71]. Previous research results have shown that the contractility of over-actin in neurons was related to the expression of MAP2 protein, one backbone protein of neuronal dendrites, which is closely related to the maturation of neurons. Therefore, maintaining the expression of MAP2 may promote neurons further maturity by stabilizing microtubule formation [72,73]. Furthermore, we investigated whether the Pd-RGO nanocomposite substrate had the ability to regulate the levels of expression of β-III tubulin, Tau-1, and MAP2 in cultured hippocampal neurons. The findings revealed that hippocampal neurons exhibited an increase in the expression of β-III tubulin, Tau-1, and MAP2 protein following the application of Pd-RGO nanocomposite treatments. Additionally, throughout the process of neural development, GAP-43, which is a particular protein found within neuronal axons, is often generated at high quantities [74–76]. Thus, its expression is regarded as one of the

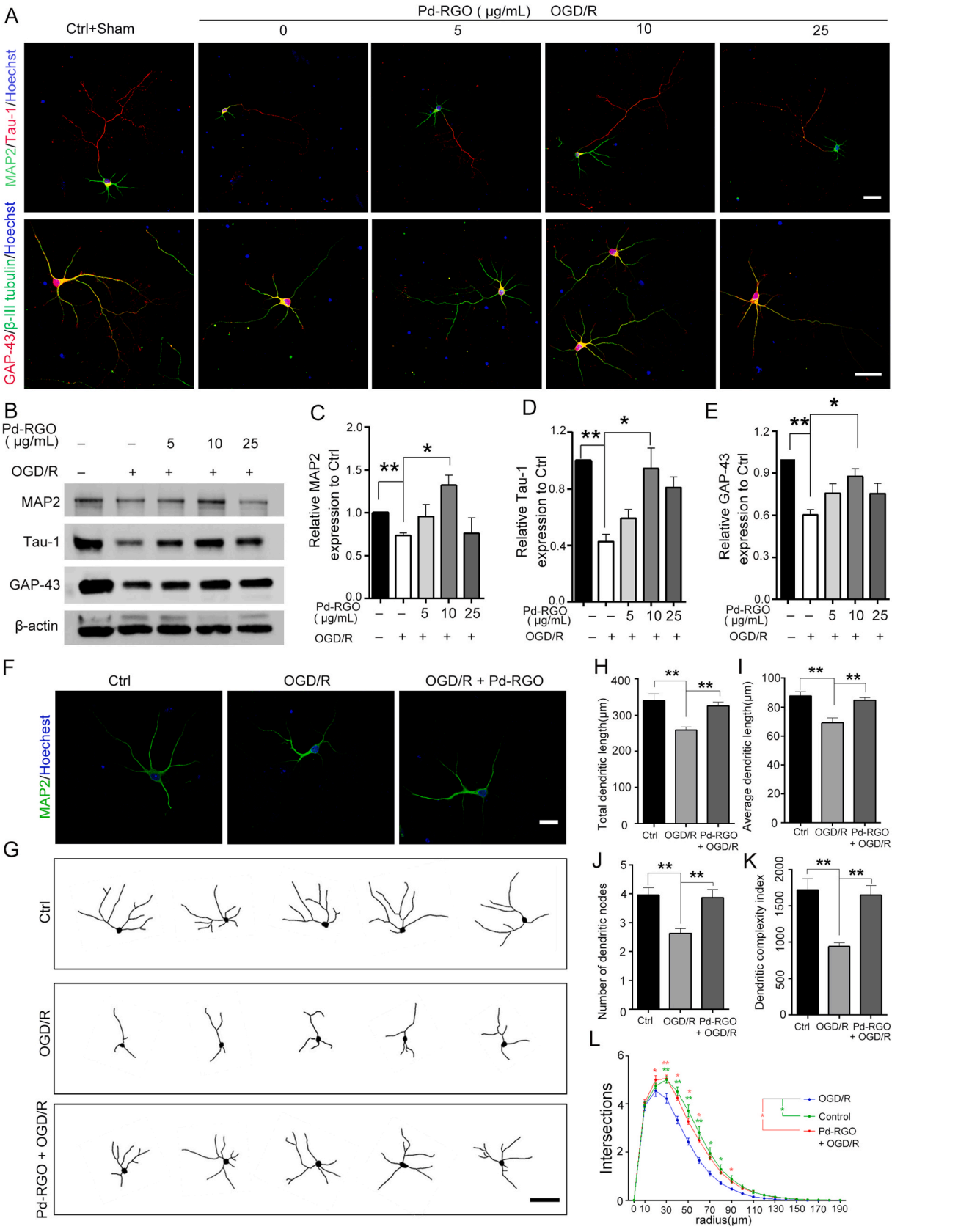

(caption on next page)

Fig. 7. Pd-RGO nanocomposite significantly facilitates dendritic outgrowth in cultured primary hippocampal neurons exposed to OGD/R. A) Representative fluorescence images of neurons exposed to OGD/R on various substrates on day 7 after seeding, neurons were immune-stained with Tau-1 (red) and MAP2 (green), Scale bar, 50 μm. And representative fluorescence images of neurons exposed to OGD/R on day 7 after seeding, neurons were immune-stained with GAP-43 (red) and β-III tubulin (green), Scale bar, 50 μm. B-E) Western blot analysis of MAP2, Tau-1 and GAP-43 in cultured hippocampal neurons exposed to OGD/R after Pd-RGO nanocomposite treated. $n = 3$–6 for each group. F) The representative fluorescence images of neurons exposed to OGD/R on the 10 μg mL^{-1} PDL-Pd-RGO nanocomposite-coated glass on day 7 after seeding, neurons were immune-stained with and MAP2 (green), Scale bar, 20 μm. G) Tracings of representative MAP2-immunolabeled neurons exposed to OGD/R on day 7 after seeding. Scale bar represented 50 μm. H–K) Quantification of total length of dendrites, average length of dendrites, number of dendritic nodes and dendritic complexity index of neurons exposed to OGD/R on the 10 μg mL^{-1} Pd-RGO nanocomposite-coated glass, which stained with dendritic marker MAP2 at DIV7. Data are expressed as mean ± SEM, $n = 80$–140 for each group, the experiment was repeated six times. L) Quantification of dendritic complexity as measured by Sholl analysis. All data are expressed as mean ± SEM, $n = 80$–140 for each group. Data were analyzed by one-way ANOVA, with *post hoc* Bonferroni tests. $^{*}p < 0.05$, $^{**}p < 0.01$, and $^{***}p < 0.001$.

important signs of neuronal axon growth and regeneration [77]. Meanwhile, GAP-43 is always used as a marker for early neurons after mitosis. Indeed, GAP-43 was related to hippocampal neuron skeletal formation and was mainly concentrated in the growth cone and presynaptic membrane of neuron axons [37,77]. More interestingly, its continuous expression is very important for maintaining the plasticity of the nervous system [38]. Finally, studies had shown that the expression of GAP-43 was related to nerve sprouting, especially to the ability of neural regeneration, under the conditions of neurological diseases [78]. Therefore, Pd-RGO nanocomposites may also affect neuronal GAP-43 expression. Our results here showed that GAP-43 expression was significantly increased in neurons after Pd-RGO nanocomposite treatments (Figs. 5–7), that seems to explain why the neurons growing on the Pd-RGO nanocomposite substrate had longer neurites.

Converging studies have reported that the surface structure of cell growth substrates affects neurite growth and determination of neuronal interactions. It had been shown that different substrates could provide different states for neuronal growth in culture hippocampal neurons [39,40]. Nowadays, the precise control of nano-roughness with nano-resolution was achieved by wet chemistry methods. Research results have shown that neurons could accurately sense and actively respond to surface changes of a few nanometers [39]. Similarly, Pd-RGO nanocomposites in our study could potentially provide a beneficial matrix for neuron growth due to its ripple-like nanomaterial surface morphology. In addition, surface chemistry cannot be ignored in promoting action between neurons and substrates [79]. Furthermore, carbon nanotubes could promote the growth of neurons due to their excellent electrical conductivity [80,81]. Therefore, it could also be speculated that one of the important factors leading to longer and more complex neurites of hippocampal neuron may be the high conductivity of Pd-RGO nanocomposite. Thus, Pd-RGO nanocomposites really lead to enhanced neurite length and complexity of neurons, probably due to the good catalytic activity and ballistic electronic conduction, but further evidence is still needed to be explored.

Neurons, like other cell types, receive complicated stimuli from their surrounding environments [82]. Although neuronal behaviors are obviously influenced by surface topography, stiffness, or physical tension, external perturbations in the extracellular matrix (ECM) always play regulatory roles in the survival, development, and functionality of neurons, as well-exemplified by soluble growth factors or proteins immobilized on the surfaces of extracellular scaffolds or other cells [83]. Neurons are encircled by three-dimensional nanostructured extracellular matrix (ECM) components, which are essential for intracellular molecular machinery and cell communication [82]. In fact, our research suggests that Pd-RGO may be a useful material for creating neural scaffolds due to its biodegradability, neuro-mimicked mechanical strength, and naturally occurring extracellular matrix (ECM) microstructure, which can provide suitable stimulation for dendritic sprouting and axonal growth. (Figs. 4 and 5). Experimental data has consistently demonstrated that 3D scaffolds provide better conditions for cell adhesion, shape, and functions than monolayer culture settings [84,85].

Current studies have revealed that neuronal neurites may shorten or even disappear when the brain suffers from ischemic injury [86,87]. Thus, neurite growth is essential for the function of the central nervous system as well as the regeneration of the neural network after injury. In this study, the primary hippocampal neurons showed a lower survival rate after OGD/R, as well as a decrease in the length and density of neuron neurites (Fig. S2), suggesting a successful OGD/R model *in vitro* [33]. As one of the important guiding clues, GAP-43 was not only one of the factors affecting the survival of neurons, but also involved in regulating the growth and branching of neuron axons [88]. Here, we carefully examined the expression of some key proteins like GAP-43 and further verified the protective effect of Pd-RGO nanocomposites on neuron after OGD/R. Thus, here we were the first to find that GAP-43 expression was up-regulated after OGD/R in cultured neurons growing on Pd-RGO nanocomposite substrates. Based on these results, Pd-RGO nanocomposites could promote the neurite growth of OGD/R-treated hippocampal neurons *in vitro*.

Since the development of nanotechnology, researchers have become increasingly interested in the remarkable capabilities of nanoparticles due to their potential in several pharmacological applications in a range of illnesses, including cerebral ischemic stroke [89]. With significant morbidity, disability, recurrence, and mortality, ischemic stroke is one of the leading causes of death worldwide, yet the available therapies are far from ideal [90]. Thus, stroke treatments are the most major unmet medical needs, and they highlight the urgent need for novel targets that have been mechanistically validated. In our study, while the research above showed that Pd-RGO nanocomposites protect neurons in OGD/R models *in vitro*, we further thoroughly assessed the *in vivo* therapeutic effectiveness of Pd-RGO nanocomposites in ischemic stroke alleviation using a rat cerebral ischemia/reperfusion damage model produced by MCAO (Figs. 8 and 9). Obviously, Pd-RGO was able to effectively alleviate ischemic stroke (Figs. 8D and 9A) with no significant damage to brain tissues. Thus, we here provide the first evidence that injection of Pd-RGO nanocomposites could greatly decrease infarct size and increase neurological functional recovery by measuring improvements in neurological impairments, locomotor coordination, asymmetry in forelimb usage, and sensorimotor activity (Fig. 8). Our results also demonstrated that the apoptosis of neurons was significantly decreased following injection of Pd-RGO nanocomposites, which may be due to the improvement of GAP43 expression within neurons (Fig. 5). The current work demonstrated a proof of concept for using Pd-RGO nanocomposites to regulate neurite outgrowth for brain protection. Further research is needed to transfer this approach into human stroke therapies [91].

Indeed, ischemia/reperfusion has complex pathogenic processes, so further mechanisms and their interactions need to be studied next. Because of their great biocompatibility, outstanding biosafety, and stable structure, as well as their ease of preparation, Pd-RGO nanocomposites have the potential to become a powerful drug-delivery neuroprotective agent for stroke in the future. Pd-RGO nanocomposites offer more alternatives for the systematic modulation of several stages in the ischemic cascade of stroke and may be employed as a safe and multipurpose neuroprotectant with outstanding practical prospects. However, Pd-RGO nanocomposites' exceptional efficacy in treating ischemic stroke may be ascribed to a number of benefits, including as their excellent biocompatibility, advantageous ECM dispersion, neuroprotection, and infarct tissue healing. Our findings suggested that it held

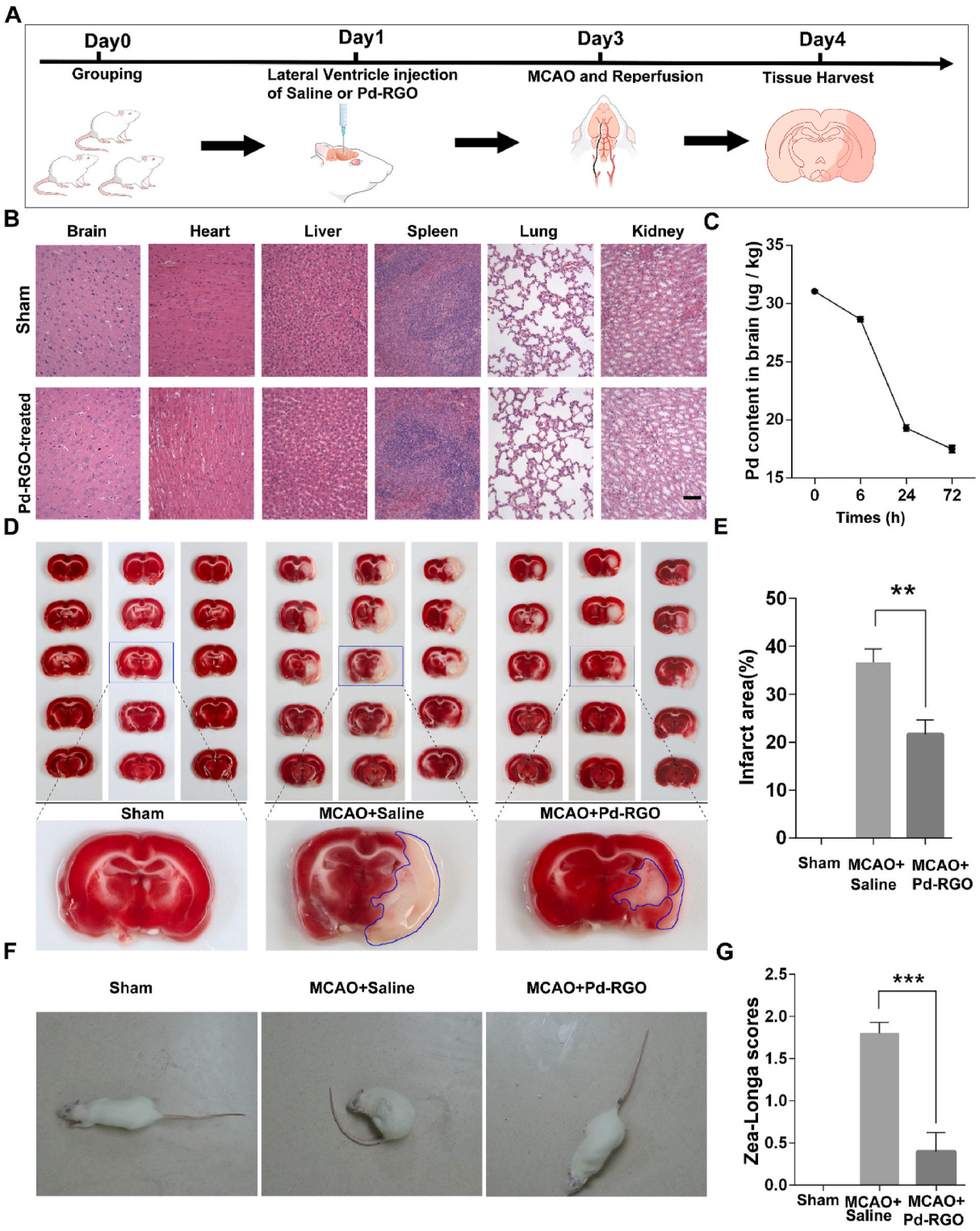

Fig. 8. Pd-RGO decrease the infarct area and improve functional results of MCAO models. A) Protocol of Pd-RGO treatment after ischemic-reperfusion injury in MCAO rats. B) Representative photomicrographs of H&E staining of different tissues as indicated. Scale bar, 100 μm. C) The dynamic changes of Pd content in the brain tissues of MCAO mice receiving Pd-RGO injection. D) Images of TTC staining with Pd-RGO treatment. Blue line indicates the infarct area in each slice. E) Statistical analysis of the ratio of the infarct area to the total brain area. F) Typical postures of the rats during neurological deficit scoring. G) Statistical analysis of the neurological deficit scoring. $^{**}p < 0.01$, $^{***}p < 0.001$. $n = 10$ for each group.

a great deal of promise as a flexible nonpharmaceutical therapy for brain ischemia/reperfusion damage.

5. Conclusion

In conclusion, a novel Pd-RGO nanocomposite with excellent biosafety capabilities was prepared here for hippocampal neurons *in vitro* and transplantation on ischemia rats *in vivo*. A series of experiments

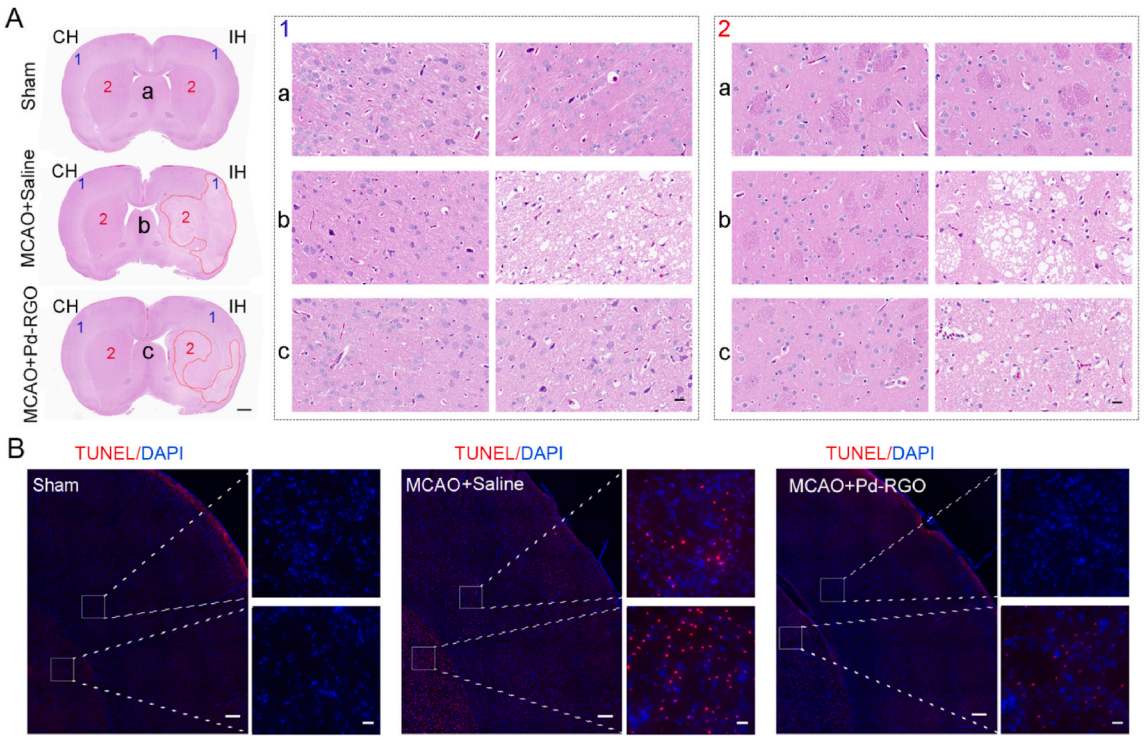

Fig. 9. Pd-RGO reduces apoptosis and cell loss caused by ischemia in rat MCAO models. A) H&E staining indicated the infarct area as well as morphological changes in cells throughout the cerebral cortex and infarct region. Scale bars, 1000 μm on the left and 20 μm on the right. B) TUNEL (red) and DAPI (blue) staining in brain sections of the rats receiving Pd-RGO or vehicle injection. Magnification for the framed area was placed on the right. Scale bars, 50 μm on the left and 20 μm on the right.

on neuron culture demonstrated that our Pd-RGO nanocomposites can enhance the growth of neuronal neurites compared with pure RGO. Comparing the two biomimetic composites, Pd-RGO was more beneficial to neurite sprouting and outgrowth *in vitro*. Importantly, it can effectively rescue OGD/R-induced injury on neuronal processes. Moreover, the neuroprotective function of Pd-RGO nanocomposites on OGD/R-injured neurons possibly mediated by increased expression of GAP-43 protein. More specific molecular mechanisms need to be further investigated in the next step. The protective effect of Pd-RGO on neurons was further verified *in vivo*. The results of transplantation treatment on MCAO rats showed that Pd-RGO significantly reduced the area of cerebral infarction, decreased apoptosis, and considerably improved the behavioral function of the animals. More research is required to determine the underlying mechanism of Pd-RGO's *in vivo* protection against apoptosis. However, this work offers a new method for creating biomimetic materials based on RGO and enhances our knowledge of the biological characteristics of biomimetic Pd-RGO composites, as well as their potential uses in biomedical and biotechnological fields, such as neural therapy. Because of interactions between these biomimetic composites and neurons, our findings suggest that the Pd-RGO nanocomposite can be used as a promising nanostructured substrate for promoting neuron growth and a nano-neuroprotectant for transplantation therapy in ischemic rats that is helpful for neural repairing. We think this kind of composites might be a viable technique utilized as implanted materials for neural tissue engineering, especially in the field of neural regenerative medicine.

CRediT authorship contribution statement

Ping Wang: Writing – original draft, Formal analysis, Data curation, Conceptualization. **Jinling Li:** Software, Methodology, Formal analysis, Conceptualization. **Shuntang Li:** Resources, Methodology, Investigation, Formal analysis. **Yuanyuan Liu:** Validation, Software, Methodology. **Jiangu Gong:** Resources, Project administration, Methodology. **Shipei He:** Software. **Weifeng Wu:** Writing – review & editing, Supervision, Methodology. **Guohe Tan:** Writing – review & editing, Visualization, Supervision. **Sijia Liu:** Writing – review & editing, Visualization, Supervision, Methodology.

Declaration of competing interest

The authors declare that they have no known competing financial interests or personal relationships that could have appeared to influence the work reported in this paper.

Data availability

Data will be made available on request.

Acknowledgements

This project was supported by grants from the Guangxi Key Technologies R&D Program (Grant number: Guike AB23026023) and National Natural Science Foundation of China (Grant numbers: 21505041, 82171200, 81860256, 82260390).

Appendix A. Supplementary data

Supplementary data to this article can be found online at https://doi.org/10.1016/j.mtbio.2024.101184.

References

[1] C.M. Madl, S.C. Heilshorn, H.M. Blau, Bioengineering strategies to accelerate stem cell therapeutics, Nature 557 (2018) 335–342.
[2] S. Shah, A. Solanki, K.B. Lee, Nanotechnology-based approaches for guiding neural regeneration, Acc. Chem. Res. 49 (2016) 17–26.
[3] G. Orive, E. Anitua, J.L. Pedraz, D.F. Emerich, Biomaterials for promoting brain protection, repair and regeneration, Nat. Rev. Neurosci. 10 (2009) 682–692.

[4] C.E. Schmidt, J.B. Leach, Neural tissue engineering: strategies for repair and regeneration, Annu. Rev. Biomed. Eng. 5 (2003) 293–347.
[5] M.V. Sofroniew, H. V, Astrocytes: biology and pathology, Acta Neuropathol. 119 (2010) 7–35.
[6] M. Mahar, V. Cavalli, Intrinsic mechanisms of neuronal axon regeneration, Nat. Rev. Neurosci. 19 (2018) 323–337.
[7] X. Gu, F. Ding, D.F. Williams, Neural tissue engineering options for peripheral nerve regeneration, Biomaterials 35 (2014) 6143–6156.
[8] J.M. Shapiro, M. L Oyen, Hydrogel composite materials for tissue engineering scaffolds, J. Occup. Med. 65 (2013) 505–516.
[9] Kenry, W.C. Lee, K.P. Loh, C.T. Lim, When stem cells meet graphene: opportunities and challenges in regenerative medicine, Biomaterials 155 (2018) 236–250.
[10] T.P. Dasari Shareena, D. McShan, A.K. Dasmahapatra, P.B. Tchounwou, A review on graphene-based nanomaterials in biomedical applications and risks in environment and health, Nano-Micro Lett. 10 (2018) 53.
[11] Y. Qu, F. He, C. Yu, X. Liang, D. Liang, L. Ma, Q. Zhang, J. Lv, J. Wu, Advances on graphene-based nanomaterials for biomedical applications, Mater. Sci. Eng., C 90 (2018) 764–780.
[12] Y. Lu, H. Lyu, A.G. Richardson, T.H. Lucas, D. Kuzum, Flexible neural electrode array based-on porous graphene for cortical microstimulation and sensing, Sci. Rep. 19 (2016) 33526.
[13] S. Goenka, V. Sant, S. Sant, Graphene-based nanomaterials for drug delivery and tissue engineering, J. Contr. Release 173 (2014) 75–88.
[14] Y. Chang, S.-T. Yang, J.-H. Liu, E. Dong, Y. Wang, A. Cao, Y. Liu, H. Wang, In vitro toxicity evaluation of graphene oxide on A549 cells, Toxicol. Lett. 200 (2011) 201–210.
[15] Y. Liao, W. Wang, X. Huang, Y. Sun, S. Tian, P. Cai, Reduced graphene oxide triggered epithelial-mesenchymal transition in A549 cells, Sci. Rep. 8 (2018) 15188.
[16] B. Zhang, H. Ni, R. Chen, T. Zhang, X. Li, W. Zhan, Z. Wang, Y. Xu, Cytotoxicity effects of three-dimensional graphene in NIH-3T3 fibroblasts, RSC Adv. (2016) 45093–45102.
[17] S.R. Ryoo, Y.K. Kim, M.H. Kim, D.H. Min, Behaviors of NIH-3T3 fibroblasts on graphene/carbon nanotubes: proliferation, focal adhesion, and gene transfection studies, ACS Nano 4 (2010) 6587–6598.
[18] E. Rozhina, S. Batasheva, A. Danilushkina, M. Kryuchkova, M. Gomzikova, Y. Cherednichenko, L. Nigamatzyanova, F. Akhatova, R. Fakhrullin, Kaolin alleviates the toxicity of graphene oxide for mammalian cells, Medchemcomm 10 (2019) 1457–1464.
[19] G. Jing, Z. Wang, X. Zhuang, X. He, H. Wu, Q. Wang, L. Cheng, Z. Liu, S. Wang, R. Zhu, Suspended graphene oxide nanosheets maintain the self-renewal of mouse embryonic stem cells via down-regulating the expression of Vinculin, Biomaterials 171 (2018) 1–11.
[20] E. Garcia-Alegria, M. Iliut, M. Stefanska, C. Silva, S. Heeg, S.J. Kimber, V. Kouskoff, G. Lacaud, A. Vijayaraghavan, K. Batta, Graphene Oxide promotes embryonic stem cell differentiation to haematopoietic lineage, Sci. Rep. 6 (2016) 25917.
[21] Y. Lu, X. Liu, D. Kuzum, Graphene-based neurotechnologies for advanced neural interfaces, Curr. Opin. Biomed. Eng. 6 (2018) 138–147.
[22] M. Antman-Passig, O. Shefi, Remote magnetic orientation of 3D collagen hydrogels for directed neuronal regeneration, Nano Lett. 16 (2016) 2567–2573.
[23] O. Akhavan, E. Ghaderi, Toxicity of graphene and graphene oxide nanowalls against bacteria, ACS Nano 4 (2010) 5731–5736.
[24] Y. Pan, N.G. Sahoo, L. Li, The application of graphene oxide in drug delivery, Expet Opin. Drug Deliv. 9 (2012) 1365–1376.
[25] M. Tang, Q. Song, N. Li, Z. Jiang, R. Huang, G. Cheng, Enhancement of electrical signaling in neural networks on graphene films, Biomaterials 34 (2013) 6402–6411.
[26] N.P. Pampaloni, D. Scaini, F. Perissinotto, S. Bosi, M. Prato, L. Ballerini, Sculpting neurotransmission during synaptic development by 2D nanostructured interfaces, Nanomedicine 14 (2018) 2521–2532.
[27] R. Weinmuellner, K. Kryeziu, B. Zbiral, K. Tav, B. Schoenhacker-Alte, D. Groza, L. Wimmer, M. Schosserer, F. Nagelreiter, S. Rösinger, M. Mildner, E. Tschachler, M. Grusch, J. Grillari, P. Heffeter, Long-term exposure of immortalized keratinocytes to arsenic induces EMT, impairs differentiation in organotypic skin models and mimics aspects of human skin derangements, Arch. Toxicol. 92 (2018) 181–194.
[28] M. Chiacchiaretta, M. Bramini, A. Rocchi, A. Armirotti, E. Giordano, E. Vázquez, T. Bandiera, S. Ferroni, F. Cesca, F. Benfenati, Graphene oxide upregulates the homeostatic functions of primary astrocytes and modulates astrocyte-to-neuron communication, Nano Lett. 18 (2018) 5827–5838.
[29] J. Song, H. Gao, G. Zhu, X. Cao, X. Shi, Y. Wang, The preparation and characterization of polycaprolactone/graphene oxide biocomposite nanofiber scaffolds and their application for directing cell behaviors, Carbon 95 (2015) 1039–1050.
[30] G. Giovannetti, P.A. Khomyakov, G. Brocks, V.M. Karpan, d. e. n. van, P.J. Kelly, Doping graphene with metal contacts, Phys. Rev. Lett. 101 (2008) 026803.
[31] H.U. Blaser, A. Indolese, A. Schnyder, H. Steiner, M. Studer, Supported palladium catalysts for fine chemicals synthesis, Journal of Molecular Catalysis A Chemical 173 (2001) 3–18.
[32] A. Sotoudeh, M. Amirmazlaghani, Graphene-based field effect diode, Superlattice. Microst. 120 (2018) 828–836.
[33] M.R. Hasan, J.H. Kim, Y.J. Kim, K.J. Kwon, C.Y. Shin, H.Y. Kim, S.H. Han, D. H. Choi, J. Lee, Effect of HDAC inhibitors on neuroprotection and neurite outgrowth in primary rat cortical neurons following ischemic insult, Neurochem. Res. 38 (2013) 1921–1934.
[34] C. Li, Y. Wu, Q. Chen, Y. Luo, P. Liu, Z. Zhou, C. Jiang, Pleiotropic microenvironment remodeling micelles for cerebral ischemia-reperfusion injury therapy by inhibiting neuronal ferroptosis and glial overactivation, ACS Nano 17 (2023) 18164–18177.
[35] R. Prakash, A. Vyawahare, R. Sakla, N. Kumari, A. Kumar, M.M. Ansari, S.S. Raza, NLRP3 inflammasome-targeting nanomicelles for preventing ischemia–reperfusion-induced inflammatory injury, ACS Nano 17 (2023) 8680–8693.
[36] W.S. Hummers, R.E. Offeman, Preparation of graphitic oxide, J. Am. Chem. Soc. 80 (1958) 1339, 1339.
[37] K.F. Meiri, P.R. Gordon-Weeks, GAP-43 in growth cones is associated with areas of membrane that are tightly bound to substrate and is a component of a membrane skeleton subcellular fraction, J. Neurosci. 10 (1990) 256–266.
[38] L.I. Benowitz, A. Routtenberg, A membrane phosphoprotein associated with neural development, axonal regeneration, phospholipid metabolism, and synaptic plasticity, Trends Neurosci. 10 (1987) 527–532.
[39] V. Brunetti, G. Maiorano, L. Rizzello, B. Sorce, S. Sabella, R. Cingolani, P.P. Pompa, Neurons sense nanoscale roughness with nanometer sensitivity, Proc. Natl. Acad. Sci. U.S.A. 107 (2010) 6264–6269.
[40] Y.-W. Fan, F.-Z. Cui, S.-P. Hou, Q.-Y. Xu, L.-N. Chen, I.S. Lee, Culture of neural cells on silicon wafers with nano-scale surface topography, J. Neurosci. Methods 120 (2002) 17–23.
[41] M. Zhou, T. Zhang, B. Zhang, X. Zhang, S. Gao, T. Zhang, Y. Lin, A DNA nanostructure-based neuroprotectant against neuronal apoptosis via inhibiting toll-like receptor 2 signaling pathway in acute ischemic stroke, ACS Nano 16 (2021) 1456–1470.
[42] E.Z. Longa, P.R. Weinstein, S. Carlson, R. Cummins, Reversible middle cerebral artery occlusion without craniectomy in rats, Stroke 1 (1989) 84–91.
[43] B. Sen, S. Kuzu, E. Demir, E. Yildirir, F. Sen, Highly efficient catalytic dehydrogenation of dimethyl ammonia borane via monodisperse palladium–nickel alloy nanoparticles assembled on PEDOT, Int. J. Hydrogen Energy 42 (2017) 23307–23314.
[44] B. Sen, A. Aygün, A. Savk, S. Akocak, F. Sen, Bimetallic palladium–iridium alloy nanoparticles as highly efficient and stable catalyst for the hydrogen evolution reaction, Int. J. Hydrogen Energy 43 (2018) 20183–20191.
[45] B. Sen, S. Kuzu, E. Demir, S. Akocak, F. Sen, Highly monodisperse RuCo nanoparticles decorated on functionalized multiwalled carbon nanotube with the highest observed catalytic activity in the dehydrogenation of dimethylamine borane, Int. J. Hydrogen Energy 42 (2017) 23292–23298.
[46] N. Lolak, E. Kuyuldar, H. Burhan, H. Goksu, S. Akocak, F. Sen, Composites of palladium–nickel alloy nanoparticles and graphene oxide for the Knoevenagel condensation of aldehydes with malononitrile, ACS Omega 4 (2019) 6848–6853.
[47] Z. Zhang, R. Xu, Z. Wang, M. Dong, B. Cui, M. Chen, Visible-light neural stimulation on graphitic-carbon nitride/graphene photocatalytic fibers, ACS Appl. Mater. Interfaces 9 (2017) 34736–34743.
[48] Z. Zhang, P. Qin, Y. Deng, Z. Ma, H. Guo, H. Guo, Y. Hou, S. Wang, W. Zou, Y. Sun, Y. Ma, W. Hou, The novel estrogenic receptor GPR30 alleviates ischemic injury by inhibiting TLR4-mediated microglial inflammation, J. Neuroinflammation 15 (2018) 206.
[49] W.C. Lee, C.H. Lim, H. Shi, L.A. Tang, Y. Wang, C.T. Lim, K.P. Loh, Origin of enhanced stem cell growth and differentiation on graphene and graphene oxide, ACS Nano 5 (2011) 7334–7341.
[50] A. K Geim, K. S Novoselov, The rise of graphene, Nat. Mater. 6 (2017) 183–191.
[51] K.F. Meiri, K.H. Pfenninger, M.B. Willard, Growth-associated protein, GAP-43, a polypeptide that is induced when neurons extend axons, is a component of growth cones and corresponds to pp46, a major polypeptide of a subcellular fraction enriched in growth cones, Proc. Natl. Acad. Sci. U. S. A. 83 (1986) 3537–3541.
[52] M. Ackermann, A. Matus, Activity-induced targeting of profilin and stabilization of dendritic spine morphology, Nat. Neurosci. 6 (2023) 1194–1200.
[53] B. Calabrese, S. Halpain, Essential role for the PKC target MARCKS in maintaining dendritic spine morphology, Neuron 48 (2005) 77–90.
[54] L.S. Minamide, A.M. Striegl, J.A. Boyle, P.J. Meberg, J.R. Bamburg, Neurodegenerative stimuli induce persistent ADF/cofilin-actin rods that disrupt distal neurite function, Nat. Cell Biol. 2 (2000) 628–636.
[55] E. Biffi, G. Regalia, A. Menegon, G. Ferrigno, A. Pedrocchi, The influence of neuronal density and maturation on network activity of hippocampal cell cultures: a methodological study, PLoS One 8 (2013) 83899.
[56] Y. Xing, L. Dai, Nanodiamonds for nanomedicine, Nanomedicine 4 (2009) 207–218.
[57] O.A. Shenderova, D.W. Brenner, Atomistic simulation of grain boundaries, triple junctions and related disclinations, Solid State Phenom. 87 (2002) 205–214.
[58] A.M. Schrand, L. Dai, J.J. Schlager, S.M. Hussain, E. Osawa, Differential biocompatibility of carbon nanotubes and nanodiamonds, Diam. Relat. Mater. 16 (2007) 2118–2123.
[59] M.T. Fitch, J. Silver, CNS injury, glial scars, and inflammation: inhibitory extracellular matrices and regeneration failure, Exp. Neurol. 209 (2008) 294–301.
[60] J.Y. Lee, C.A. Bashur, A.S. Goldstein, C.E. Schmidt, Polypyrrole-coated electrospun PLGA nanofibers for neural tissue applications, Biomaterials 30 (2009) 4325–4335.
[61] Y.J. Chang, C.M. Hsu, C.-H. Lin, M.-S. Lu, L. Chen, Electrical stimulation promotes nerve growth factor-induced neurite outgrowth and signaling, Biochim. Biophys. Acta 1830 (2013) 4130–4136.
[62] Y. Huang, Y. Li, J. Chen, H. Zhou, S. Tan, Electrical stimulation elicits neural stem cells activation: new perspectives in CNS repair, Front. Hum. Neurosci. 9 (2015) 586–595.

[63] E.D. Kenny, R.S. Paredes, L.A. de Lacerda, Y.C. Sica, G.P. de Souza, J. Lázaris, Artificial neural network corrosion modeling for metals in an equatorial climate, Corrosion Sci. 51 (2009) 2266–2278.
[64] B. Kim, S. Kim, H. Kim, Effects of alloying elements (Cr, Mn) on corrosion properties of the high-strength steel in 3.5% NaCl solution, Adv. Mater. Sci. Eng. 2018 (2018).
[65] N. Alegret, A. Dominguez-Alfaro, J.M. González-Domínguez, B. Arnaiz, U. Cossío, S. Bosi, E. Vázquez, P. Ramos-Cabrer, D. Mecerreyes, M. Prato, Three-dimensional conductive scaffolds as neural prostheses based on carbon nanotubes and polypyrrole, ACS Appl. Mater. Interfaces 10 (2018) 43904–43914.
[66] X. Liu, A.L. Miller, S. Park, B.E. Waletzki, Z. Zhou, A. Terzic, L. Lu, Functionalized carbon nanotube and graphene oxide embedded electrically conductive hydrogel synergistically stimulates nerve cell differentiation, ACS Appl. Mater. Interfaces 9 (2017) 14677–14690.
[67] P. Gupta, A. Agrawal, K. Murali, R. Varshney, S. Beniwal, S. Manhas, P. Roy, D. Lahiri, Differential neural cell adhesion and neurite outgrowth on carbon nanotube and graphene reinforced polymeric scaffolds, Mater. Sci. Eng., C 97 (2019) 539–551.
[68] A.B. Kaiser, V. Skákalová, Electronic conduction in polymers, carbon nanotubes and graphene, Chem. Soc. Rev. 40 (2011) 3786–3801.
[69] A.A. Balandin, Thermal properties of graphene and nanostructured carbon materials, Nat. Mater. 10 (2011) 569–581.
[70] S.L. Rogers, P.C. Letourneau, S.L. Palm, J. McCarthy, L.T. Furcht, Neurite extension by peripheral and central nervous system neurons in response to substratum-bound fibronectin and laminin, Dev. Biol. 98 (1983) 212–220.
[71] G.V. Johnson, R.S. Jope, The role of microtubule-associated protein 2 (MAP-2) in neuronal growth, plasticity, and degeneration, J. Neurosci. Res. 33 (1992) 505–512.
[72] G.H. Poplawski, A.K. Tranziska, I. Leshchyns'ka, I.D. Meier, T. Streichert, V. Sytnyk, M. Schachner, L1CAM increases MAP2 expression via the MAPK pathway to promote neurite outgrowth, Mol. Cell. Neurosci. 50 (2012) 169–178.
[73] B. Shafit-Zagardo, N. Kalcheva, Making sense of the multiple MAP-2 transcripts and their role in the neuron, Mol. Neurobiol. 16 (1998) 149–162.
[74] C.-C. Chang, C.H. Tien, E.J. Lee, W.S. Juan, Y.-H. Chen, Y.-C. Hung, T.-Y. Chen, H.-Y. Chen, T.-S. Wu, Melatonin inhibits matrix metalloproteinase-9 (MMP-9) activation in the lipopolysaccharide (LPS)-stimulated RAW 264.7 and BV2 cells and a mouse model of meningitis, J. Pineal Res. 53 (2012) 188–197.
[75] O. Bozdagi, V. Nagy, K.T. Kwei, G.W. Huntley, In vivo roles for matrix metalloproteinase-9 in mature hippocampal synaptic physiology and plasticity, J. Neurophysiol. 98 (2007) 334–344.
[76] B.Z. Barkho, A.E. Munoz, X. Li, L. Li, L.A. Cunningham, X. Zhao, Endogenous matrix metalloproteinase (MMP)-3 and MMP-9 promote the differentiation and migration of adult neural progenitor cells in response to chemokines, Stem Cell. 26 (2008) 3139–3149.
[77] J.H. Skene, Axonal growth-associated proteins, Annu. Rev. Neurosci. 12 (1989) 127–156.
[78] E.R. Chapman, D. Au, K.A. Alexander, T.A. Nicolson, D.R. Storm, Characterization of the calmodulin binding domain of neuromodulin, J. Biol. Chem. 266 (1991) 207–213.
[79] L.A. Cyster, D.M. Grant, K.G. Parker, T.L. Parker, The effect of surface chemistry and structure of titanium nitride (TiN) films on primary hippocampal cells, Biomol. Eng. 19 (2002) 171–175.
[80] E.B. Malarkey, K.A. Fisher, E. Bekyarova, W. Liu, R.C. Haddon, V. Parpura, Conductive single-walled carbon nanotube substrates modulate neuronal growth, Nano Lett. 9 (2009) 264–268.
[81] A. Fabbro, S. Bosi, L. Ballerini, M. Prato, Carbon nanotubes: artificial nanomaterials to engineer single neurons and neuronal networks, ACS Chem. Neurosci. 3 (2012) 611–618.
[82] R.K. Upadhyay, Role of regeneration in tissue repairing and therapies, J. Regen. Med. Tissue Eng. 4 (2015).
[83] S.J. Franco, U. Müller, Extracellular matrix functions during neuronal migration and lamination in the mammalian central nervous system, Dev. Neurobiol. 71 (2011) 889–900.
[84] K.P. Das, T.M. Freudenrich, W.R. Mundy, Assessment of PC12 cell differentiation and neurite growth: a comparison of morphological and neurochemical measures, Neurotoxicol. Teratol. 26 (2004) 397–406.
[85] I.M. El-Sherbiny, M.H. Yacoub, Hydrogel scaffolds for tissue engineering: progress and challenges, Glob. Cardiol. Sci. Pract. 2013 (2013) 316–342.
[86] J. Chen, A. Zacharek, X. Cui, A. Shehadah, H. Jiang, C. Roberts, M. Lu, M. Chopp, Treatment of stroke with a synthetic liver X receptor agonist, TO901317, promotes synaptic plasticity and axonal regeneration in mice, J. Cerebr. Blood Flow Metabol. 30 (2010) 102–109.
[87] M.L. Hendrickson, C. Ling, R.E. Kalil, Degeneration of axotomized projection neurons in the rat dLGN: temporal progression of events and their mitigation by a single administration of FGF2, PLoS One 7 (2012) e46918.
[88] M.R. Holahan, A shift from a pivotal to supporting role for the growth-associated protein (GAP-43) in the coordination of axonal structural and functional plasticity, Front. Cell. Neurosci. 11 (2017) 266–285.
[89] Z. Huang, K. Qian, J. Chen, Y. Qi, E. Yifeng, J. Liang, L. Zhao, A biomimetic zeolite-based nanoenzyme contributes to neuroprotection in the neurovascular unit after ischaemic stroke via efficient removal of zinc and ROS, Acta Biomater. 144 (2022) 142–156.
[90] W. Gao, J. He, L. Chen, X. Meng, Y. Ma, L. Cheng, X. Yan, Deciphering the catalytic mechanism of superoxide dismutase activity of carbon dot nanozyme, Nat. Commun. 14 (2023) 160.
[91] S. Zhang, X. Zhang, H. Zhong, X. Li, Y. Wu, J. Ju, S.T. Hou, Hypothermia evoked by stimulation of medial preoptic nucleus protects the brain in a mouse model of ischaemia, Nat. Commun. 13 (2022) 6890.